TIM-4 Identifies Effector B Cells Expressing a RORγt-Driven Proinflammatory Cytokine Module That Promotes Immune Responsiveness

Qing Ding[1], Yufan Wu[2], Elena Torlai Triglia[2], Jennifer L. Gommerman[3], Ayshwarya Subramanian[2,4], Vijay K. Kuchroo[2,4,5], and David M. Rothstein[1,6*]

[1]Thomas E. Starzl Transplantation Institute; University of Pittsburgh School of Medicine, Pittsburgh, PA, USA.

[2]Klarman Cell Observatory, Broad Institute of MIT and Harvard; Cambridge, MA, USA

[3] Dept. Of Immunology, University of Toronto; Toronto ON, Canada.

[4]The Broad Institute of MIT and Harvard; Cambridge, MA, USA.

[5]Gene Lay Institute of Immunology and Inflammation, Harvard Medical School and Brigham and Women's Hospital, Boston, MA, USA.

[6]Department of Immunology, University of Pittsburgh School of Medicine, Pittsburgh, PA 15261, USA.

*Corresponding author: Rothsteindm@upmc.edu

ABSTRACT

B cells can express pro-inflammatory cytokines that promote a wide variety of immune responses. Here we show that B cells expressing the phosphatidylserine receptor TIM-4, preferentially express IL-17A, as well as IL-22, IL-6, IL-1β, and GM-CSF - a collection of cytokines reminiscent of pathogenic Th17 cells. Expression of this proinflammatory module requires IL-23R signaling and selective expression of RORγt and IL-17A by TIM-4$^+$ B cells. TIM-4$^+$ B cell-derived-IL-17A not only enhances the severity of experimental autoimmune encephalomyelitis (EAE) and promotes allograft rejection, but also acts in an autocrine manner to prevent their conversion into IL-10-expressing B cells with regulatory function. Thus, IL-17A acts as an inflammatory mediator and also enforces the proinflammatory activity of TIM-4$^+$ B cells. Thus, TIM-4 serves as a broad marker for RORγt$^+$ effector B cells (Beff) and allows further study of the signals regulating Beff differentiation and effector molecule expression.

INTRODUCTION

In addition to a primary role in humoral immunity, B cells are potent regulators of the immune response through antigen presentation, co-receptor engagement and production of cytokines[1-6]. Regulatory B cells (Bregs) inhibit immune responses through the expression of suppressive cytokines and coinhibitory molecules[4-7]. The phosphatidylserine receptor, TIM-1, is both a broad and functional marker for Bregs that play an essential role in restraining tissue inflammation and maintaining self-tolerance[7,8]. In addition to being a marker of Breg identity, TIM-1 signaling regulates the expression of a "regulatory module" that includes IL-10 and various coinhibitory molecules including TIGIT[7]. As such, specific deletion of TIM-1 in B cells results in spontaneous systemic autoimmunity characterized by inflammatory infiltration of multiple organs and accompanied by dermatitis, weight loss/rectal prolapse, and EAE-like paralytic disease.

In contrast to Bregs, effector B cells (Beffs), express proinflammatory cytokines that promote anti-microbial responses, autoimmunity, and allograft and tumor rejection[2,5,6,9]. For example, B cell-derived IL-2 and TNFα are required for clearance of *H. polygyrus* infection[10]. B cell-derived IL-6 enhances Th1 and Th17 responses and increases the severity of EAE[11,12] (a model of human multiple sclerosis), and B cell-derived IFNγ promotes Th1 and inhibits Treg responses essential for generation of proteoglycan-induced arthritis[11,12]. During *T. Cruzii* infection, a pathogen-associated trans-sialidase was reported to specifically induce IL-17A expression in B cells through a RORγt-independent mechanism, promoting pathogen clearance[13]. However, a broader characterization and role for IL-17A in Beff function has not been elucidated. In humans, GM-CSF produced by B cells has been implicated in multiple sclerosis[14,15]. B cell depletion with anti-CD20 reduces T cell hyperreactivity and is now the treatment of choice for relapsing multiple sclerosis.

Unlike Bregs, the phenotype of Beffs has not been well-studied and this has impeded our understanding of their generation and effector functions. We previously showed that TIM-4$^+$ B cells are enriched for IFNγ and enhance tumor and allograft rejection in vivo – activity opposite to

that of TIM-1+ Bregs[9]. However, no more broadly unifying marker for Beffs has been identified and it remains unclear whether B cells expressing different inflammatory cytokines are related in phenotype or are regulated by common signaling mechanisms. It is also unknown whether Bregs and Beffs bear any functional relationship. Here, we characterize the role of TIM-4$^+$ B cells as Beffs using high-throughput sequencing and murine models of autoimmunity and transplantation. We show that in addition to IFNγ, TIM-4$^+$ B cells express a unique pro-inflammatory module driven by RORγt expression that includes IL-17A and additional proinflammatory cytokines in a pattern resembling pathogenic Th17 cells. B cell-derived IL-17A is not only a potent driver of inflammatory responses but is required as an autocrine factor to enforce expression of the proinflammatory module by TIM-4$^+$ Beffs and prevent their conversion into IL-10-expressing B cells with regulatory function. Thus, TIM-4 is a marker that integrates B cells with many of the inflammatory functions previously ascribed to Beffs, and we identify a dual role for IL-17A as both a proinflammatory cytokine and regulator of Beff versus Breg function.

RESULTS

TIM-4$^+$ B cells express IL-17A

As previously shown, TIM-4 is expressed on a subset of splenic B cells similar in size but largely distinct from TIM-1$^+$ B cells (**Fig. 1A)**[9]. In addition to IFNγ production, we now show that TIM-4$^+$ B cells from alloimmunized mice are also enriched for IL-17A production compared to total (CD19+) B cells or TIM-1$^+$ B cells (**Fig. 1B-C**), and given their relatively low frequency of IL-10 expression, TIM-4$^+$ B cells have a markedly higher IL-17A:IL-10 ratio than TIM-1$^+$ B cells (**Fig. 1B-D**). In contrast, most B cells lack both TIM-1 and TIM-4 (double negative; DN) and produce minimal IL-10, IL-17A or IFNγ (**Fig. 1B** and [9]). Most B cell-derived IL-17A is produced by the TIM-4$^+$ subset, as confirmed by staining B cells from alloimmunized IL-17A GFP-reporter mice for TIM-4 in the absence or presence of *in vitro* stimulation with PMA and ionomycin plus brefeldin A ("PIB") for 5 hours to enhance cytokine expression (**Fig. 1E; Supplementary Fig. 1A** shows B cell gating

strategy). Similar levels of IL-17A were observed after immunization of mice for EAE (MOG_{35-55}, CFA, and pertussis toxin), suggesting that IL-17A production is a generalized response by a portion of TIM-4^+ B cells to immunizing stimuli (**Supplementary Fig. 1B, C**). To determine whether IL-17A production could be enhanced *in vitro*, sort-purified $CD19^+$ B cells from naïve IL-17-EGFP reporter mice were stimulated with anti-IgM for 24 hours with or without the addition of various cytokines. After culture, bright EGFP-fluorescence was observed on a subset of B cells marked by the activation antigen Sca-1, and EGFP expression was increased 8-12-fold by the addition of IL-23 (**Supplementary Fig. 2A, B**). IL-1β increased IL-17A production to a lesser degree but had a synergistic effect when combined with IL-23. IL-6 had a small additive effect. To corroborate IL-17A production by intracellular staining and reporter expression, we examined cytokine secretion. TIM-4^+ B cells stimulated for 48 hours with anti-IgM secrete IL-17A, but only in the presence of IL-23 (**Fig. 1F)**. In contrast, TIM-4^- B cells did not secrete detectable IL-17A. Finally, TIM-4^+ but not TIM-4^- B cells express IL-17A mRNA after stimulation with anti-IgM plus IL-23 (**Supplementary Fig. 2C**). Thus, TIM-4^+ B cells express IL-17A and this was enhanced *in vitro* by IL-23.

B cell IL-17A is an important driver of allo- and auto- immune responses

To determine the role of IL-17A produced by B cells on the immune response, we examined EAE in μMT mice receiving adoptive transfer of WT versus *Il17a*$^{-/-}$ B cells. In agreement with previous studies, μMT mice exhibit severe and unremitting EAE induced by MOG_{35-55} peptide, and this is reduced by the transfer of WT B cells which have been shown to contain Bregs (**Fig. 2A**)[16]. We reasoned that since WT B cells may not only include Bregs, but also IL-17A-producing Beffs, transfer of *Il17a*$^{-/-}$ B cells might further reduce EAE severity. Indeed, transfer of *Il17a*$^{-/-}$ B cells into μMT mice significantly reduced the severity of EAE well below that seen after transfer of WT B cells.

We next wished to confirm the activity of Il17a$^{-/-}$ B cells in an allograft setting which results in a robust innate and polyclonal T cell response [17,18]. To remove the potentially confounding influence of Bregs from the findings, we transferred sort-purified TIM-4^{+} Beffs from alloimmunized syngeneic (B6) mice into chemically diabetic μMT (B6) islet allograft recipients. As we previously demonstrated, transfer of WT TIM-4^{+} B cells accelerated islet allograft rejection compared to control μMT recipients without B cell transfer (**Fig. 2B**). Surprisingly, *Il17a*$^{-/-}$ TIM-4^{+} B cells from alloimmunized mice not only failed to accelerate graft rejection, but markedly prolonged graft survival. In attempts to explain the suppressive activity of TIM-4^{+} B cells from *Il17a*$^{-/-}$ mice, we examined their cytokine expression. Compared to WT B cells, those from *Il17a*$^{-/-}$ mice produced IL-10 with twice the normal frequency (**Fig. 2C, D**). In particular, IL-10 frequency amongst *Il17a*$^{-/-}$ TIM-4^{+} B cells increased 3-fold, now similar to that of WT TIM-1^{+} B cells (**Fig. 1**).

To ensure that the effect on B cell IL-10 observed above was not due to dysregulation of B cells arising in globally IL-17A-deficient mice, we generated mixed bone marrow (BM) chimeras where B cells specifically lacked IL-17 (lethally irradiated μMT mice reconstituted with a 1:5 mixture of *Il17a*$^{-/-}$ plus μMT bone marrow). B cell *Il17a*$^{-/-}$ BM chimeras exhibited prolonged islet allograft survival with 33% of recipients never rejecting their allografts (**Fig. 2E**). In contrast, control uMT BM chimeras with WT B cells (reconstituted with a 1:5 mixture of WT plus μMT marrow) or uMT BM allograft recipients (reconstituted with 100% μMT BM), both acutely rejected islet allografts (**Fig 2E**) with a tempo similar to unmodified naive μMT allograft recipients (**Fig 2B**). We also generated mixed bone marrow (BM) chimeras where B cells specifically lacked lacked *Rorc* (encoding RORγt) by reconstituting lethally irradiated μMT hosts with a 1:5 mixture of *Rorc*$^{-/-}$ plus μMT BM. Compared to control μMT BM chimeras with WT B cells, B cells from *Rorc*$^{-/-}$ BM chimeras produced markedly reduced IL-17A (**Fig. 2E**). This demonstrates that like T cells, B cell IL-17 is RORγt dependent. Similar to B cell *Il17a*$^{-/-}$ BM chimeras, these B cell *Rorc*$^{-/-}$ BM chimeric

mice also exhibited prolonged islet allograft survival with 30% of recipients never rejecting their allografts (**Fig. 2E**).

Endogenous $CD4^+$ T cells in B cell IL-17A-deficient chimeras expressed significantly less IL-17A and IFNγ, and although IL-10 was not increased, there was a 2-fold increase in $FOXP3^+$ Tregs (**Fig. 2F**). To determine how IL-17A-deficient B cells alter an antigen-specific T cell response within the context of an alloimmune response, B cell *Il17a*$^{-/-}$ BM chimeras vs. WT B cell control BM chimeras were immunized with Act-mOva.BALB/c.B6 F1 splenocytes, followed by adoptive transfer of CFSE-labelled OTII $CD4^+$ T cells[19,20]. IL-17A-deficiency in B cells was associated with decreased proliferation (day 4) and altered frequency of cytokine production (day 7) by OTII $CD4^+$ T cells. This included a 2-fold decrease in IFNγ, and $\geq$1.7-fold increase in IL-10 and IL-4 (**Supplementary Fig. 3A**). Similar changes were observed in transferred $CD8^+$ OT-1 cells (**Supplementary Fig. 3B**). Thus, in the absence of Beff-derived IL-17A, T cell proliferation was decreased, and the T cell response was skewed towards less inflammatory and more regulatory activity. Examination of endogenous B cells in alloimmunized *Il17a*$^{-/-}$ BM chimeras versus WT B cell control BM chimeras demonstrated that, as expected, B cell IL-17A was negligible, but IFNγ was also reduced by ~30%, and once again B cell-derived IL-10 was increased more than 2-fold (**Fig. 2F**).

In a further attempt to separate IL-17/RORγt deficiency from increased IL-10, we generated mice with an inducible knockout of *Rorc* in B cells by crossing *hCd20-ERT2.Cre* and *Rorc*$^{fl/fl}$ mice (RORγt-iBKO). These mice are entirely normal until being placed on Tamoxifen (TAM) chow to acutely induce B cell-specific deletion of RORγt. In comparison to TAM-treated *Rorc*$^{fl/fl}$ (Flox control) mice, B cells from RORγt-iBKO mice exhibited an 80% reduction in B cell-derived IL-17A (**Fig. 2G)**. RORγt-iBKO mice exhibited prolongation of islet allograft survival compared to either Flox control or *hCd20-ERT2.Cre* (Cre control) mice, with ~35% surviving long-term (**Fig. 2H**), very

similar to that seen in the B cell *Il17a*$^{-/-}$ or *Rorc*-/- BM chimeras above. Furthermore, RORγt-iBKO mice also exhibited significantly decreased EAE severity (**Supplementary Fig. 3C**). Analysis of B cells in alloimmunized RORγt-iBKO mice again demonstrated increased frequency of IL-10 production, ~2-fold by total B cells and 5-fold by TIM-4^{+} B cells (**Fig. 2I and Supplementary Fig. 3D**). Thus, even the acute loss of RORγt and IL-17A in developmentally normal mice results in dysregulated IL-10 production in the TIM-4^{+} Beff subset. Furthermore, the loss of proinflammatory IL-17A and increased IL-10 production by B cells is associated with increased allograft survival and decreased EAE severity.

Regulation of IL-17A and IL-10 expression in B cells by IL-23 and IL-17

The data above (**Figs. 1 and S2**) suggested that IL-17A production by TIM-4^{+} B cells is IL-23-dependent while *Il17* or *Rorc* deletion in B cells, augments IL-10 production. To gain further insight into the regulation of these cytokines, we examined *Il17a* and *Il10* expression at the transcriptional level by performing quantitative PCR (qPCR) on sort-purified TIM-4^{+}(TIM-1^{-}) and TIM-1^{+}(TIM-4^{-}) B cells from WT or *Il23r*$^{-/-}$ mice after anti-IgM stimulation with or without additional cytokines for 24 hours. Stimulation of TIM-4^{+} B cells with anti-IgM induced detectable *Il17a* mRNA, and this was increased ~3-fold with the addition of IL-17A and ~10-fold with IL-23 (**Fig. 3A**). Consistent with reporter expression (**Supplementary Fig. 2B**), IL-1β synergized with IL-23 in augmenting *Il17a* mRNA (**Fig. 3A**). Neutralizing IL-17 in the culture by adding anti-IL-17A mAb decreased *Il17a* mRNA expression induced by either IL-23 alone or IL-23 combined with IL-1β, suggesting that part of the effect of IL-23 on increased IL-17A transcription is mediated by IL-17A secreted into the medium in a positive feedback loop. TIM-4^{+} B cells from *Il23r*$^{-/-}$ mice exhibited markedly reduced *Il17a* expression, confirming the requirement for IL-23 signaling to induce *Il17a* expression by TIM-4^{+} B cells (**Fig. 3A**). In contrast, neither WT nor *Il23r*$^{-/-}$ TIM-1^{+} B cells expressed detectable *Il17a* mRNA. The mRNA expression data was confirmed at the protein level by comparing IL-17A secretion by sort-purified TIM-1^{+} versus TIM-

4^+ B cells *in vitro* after 48-hour culture (**Fig. 3B**). IL-23 markedly enhances IL-17A secreted by anti-IgM-treated TIM-4^+ B cells. As expected, anti-IL-17A completely neutralized IL-17A detected in the supernatants. TIM-1^+ B cells secrete minimal IL-17A even after IL-23 treatment.

Our data (**Fig. 2** and **Supplementary Fig. 3**) indicate that deletion of either *Rorc* or *Il17a* in B cells increases IL-10 production by TIM-4^+ B cells. This suggests that B cell-derived IL-17A directly or indirectly inhibits IL-10 and maintains Beff function. To address this, we examined IL-10 secretion by sort-purified TIM-4^+ versus TIM-1^+ B cells *in vitro*. Anti-IgM-stimulated TIM-4^+ B cells secrete only 17% as much IL-10 as TIM-1^+ B cells (**Fig. 3C**), in agreement with the frequency of IL-10 expression determined by intracellular staining (**Fig. 1**). The addition of IL-23 to TIM-4^+ B cells, which promotes IL-17A secretion, inhibits their secretion of IL-10 ~3-fold. However, when IL-17A in the supernatant is neutralized with anti-IL-17A, anti-IgM plus IL-23-stimulated TIM-4^+ B cells increase their IL-10 secretion almost 8-fold (~2.5-fold above the baseline with anti-IgM alone; **Fig. 3C**). In contrast, IL-10 secretion after anti-IgM plus IL-23 treatment is further reduced by the addition of exogenous IL-17A. These data suggest that IL-17A directly inhibits IL-10 secretion by TIM-4^+ B cells and contributes to the inhibitory effect of IL-23.

TIM-1^+ B cells secrete higher levels of IL-10 in response to anti-IgM than TIM-4^+ B cells and IL-10 production is markedly inhibited by IL-23 (**Fig. 3C**). While IL-23 induces detectable IL-17A secretion by TIM-1^+ B cells (**Fig. 3B**), this is unlikely to be the main mechanism by which IL-23 inhibits IL-10 production in TIM-1^+ B cells since IL-17A neutralization only slightly restores IL-10, and addition of exogenous IL-17A has no significant effect on IL-10 secretion compared to IL-23 alone (**Fig. 3C**). Thus, IL-23 does signal and inhibit IL-10 secretion in both TIM-1^+ and TIM-4^+ B cells. However, in TIM-4^+ B cells the inhibition of IL-10 by IL-23 signaling can be overcome by IL-17A neutralization, whereas in TIM-1^+ B cells IL-23-mediated suppression of IL-10 appears largely independent of IL-17A.

Examination of *Il10* mRNA by qPCR generally corroborates cytokine secretion data (**Fig. 3D**). Neutralization of IL-17 in IL-23 treated B cells augmented *Il10* expression, particularly in the TIM-4+ subset which expresses more IL-17. *Il23r*$^{-/-}$ TIM-4+ and TIM-1+ B cells both expressed more *Il10* than their WT counterparts but did not respond to IL-17 neutralization, consistent with their lack of IL-17 expression (**Fig. 3A, D**). Yet, addition of exogenous IL-17A reduced IL-10 expression in TIM-4+ and TIM-1+ B cells, even in the absence of IL-23 signaling. Taken together, our data indicate that IL-17A has direct and independent effects to suppress *Il10* expression in both TIM-4+ and TIM-1+ B cells. Since B cells from BM chimeras specifically lacking B cell-derived IL-17 exhibit increased IL-10 production (**Fig. 2D)**, our findings suggest that B cell-derived IL-17A acts as an autocrine factor to suppress B cell IL-10. If IL-17A has a direct effect on B cell *Il10* expression, IL-17R-deficient B cells should express more *Il10*. To test this, we generated *Il17RC*$^{fl/fl}$ X CD19-Cre (IL-17RC BKO) mice and compared these to CD19-Cre controls. Consistent with our hypothesis, B cells from immunized IL-17RC BKO mice produced over 40% more IL-10 than Cre control B cells (**Fig. 3E**).

IL-17A production in TIM-4+ vs. TIM-1+ B cells is due to selective expression of RORγt.

Both TIM-1+ and TIM-4+ B cells respond to IL-17 and IL-23 with reduced IL-10 expression, however, only TIM-4+ B cells respond with increased IL-17 expression. Thus, these two distinct subsets of B cells exhibit major differences in response to cytokines regulating their effector function. In this regard, we demonstrated above that B cell IL-17 expression is dependent on RORγt. Therefore, we asked whether differences in RORγt levels might underlie the major difference in regulation of cytokine expression by TIM-4+ vs. TIM-1+ B cells. RORγt is almost exclusively expressed by TIM-4+ B cells and this correlates directly with IL-17A expression (**Fig 4 A,B**). Only a very small fraction of DN or TIM-1+ B cells express RORγt or IL-17, and this is at low MFI. RORγt is expressed in ~3% of TIM-4+ B cells from naïve mice and increased in

frequency to 5% after alloimmunization (**Supplementary Fig 4A**). In vitro stimulation (PIB) further increases RORγt expression on TIM-4+ B cells (compare **Supplementary Fig 4B and Fig 4B**).

Consistent with intracellular staining (**Fig. 2G**) B cells from TAM-treated RORγt iBKO mice exhibit significantly reduced IL-17A secretion in response to anti-IgM. Moreover, RORγt deletion essentially abrogated the increase in IL-17A secretion induced by IL-23 compared to Cre-control mice (**Fig 4C)**. Low level expression of IL-17A secretion is consistent with incomplete deletion of RORγt in these iBKO mice. Also consistent with intracellular staining (**Supplementary Fig. 3D**), deletion of RORγt from RORγt iBKO mice, resulted in increased IL-10 secretion by TIM-4+ B cells (**Fig 4D**). Notably, exogenous IL-23 reduced IL-10 secretion by TIM-4+ B cells lacking RORγt, suggesting that IL-23 does exert an IL-17-independent effect. Although exogenous IL-17 inhibits IL-10 secretion by RORγt-deficient TIM-4+ B cells, IL-10 remained far higher than by Cre-control TIM-4+ B cells. This suggests that RORγt inhibits IL-10 secretion through other means. In this regard, we previously showed that RORγt can bind to the IL-10 promotor and suppress IL-10 expression in Th17 cells [21].

Profiling TIM-4$^+$B cells reveals expression of multiple pro-inflammatory cytokines in a pattern resembling pathogenic Th17 cells

Based on their expression of RORγt, we asked whether TIM-4$^+$ B cells expressed additional pro-inflammatory cytokines, in comparison to the anti-inflammatory profile of TIM-1$^+$ B cells. To address this, we performed population level transcriptomic sequencing (RNA-seq) on RNA isolated from highly sort-purified TIM-4$^+$(TIM-1$^-$), TIM-1$^+$(TIM-4$^-$), and TIM-4$^-$TIM-1$^-$ (DN) B cells from spleens of alloimmunized mice stimulated for 24 hours with anti-IgM plus IL-23. This allowed us to compare TIM-4$^+$ Beffs and TIM-1$^+$ Bregs, separately from the majority DN B cell population which expresses little IL-17, IFNγ, or IL-10 (**Fig. 1** and [9]).

Principal component analysis (PCA) revealed that PC1 separated the expression profiles of TIM-1$^+$ and TIM-4$^+$ B cells, while PC2 separated DN B cells from both TIM-4$^+$ and TIM-1$^+$ B cells (**Supplementary Fig. 5A**). Variability in TIM-1$^+$ samples from different mice along PC1 related to total number of unique genes detected. Comparison of TIM-4$^+$ and TIM-1$^+$ B cells by differential gene expression analysis revealed 3425 upregulated genes (613 with fold change >1.5) and 7858 downregulated genes (7393 with fold change >1.5) in the TIM-4$^+$ population (FDR <0.05; **Fig. 5A)**. Genes of interest are displayed in the volcano plot (**Fig. 5B)**. Compared to TIM-1$^+$ B cells, TIM-4$^+$ B cells not only expressed higher levels of *Il17a*, but also a pro-inflammatory module comprising *Il17f, Il22, Csf2, Il6, Il1β, TNFα,* and *Il2* **(Fig. 5B-D**). These transcripts were not detected in the absence of IL-23 (not shown). As expected, TIM-1$^+$ cells expressed more *Il10*, and also *Ctla4, Nte5* (expressing CD73), *ENTpd1* (expressing CD39), *Cd274* (expressing PD-L1), and *Pdcd1lg2* (expressing PD-L2)[7]. Of note, *Ifng* expression, showed a trend, but was not statistically higher in TIM-4$^+$ B cells (**Fig. 5C**), even though IFNγ protein expression is higher in freshly isolated TIM-4$^+$ versus TIM-1$^+$ B cells[9]. Surprisingly, in these stimulated cells, the TIM-4 gene (*Timd4*) was expressed at higher levels by TIM-1$^+$ B cells even though TIM-4 protein was not detected by flow cytometry. Many of the same proinflammatory cytokines noted above were also increased in TIM-4$^+$ B cells compared to DN B cells (**Fig. 5C, D**). The top 50 upregulated and downregulated genes in TIM-4$^+$ vs TIM-1$^+$ B cells are listed in **Table S1.** Intracellular staining confirms increased expression of IL-1β, GM-CSF, IL-22, and IL-6 at the protein level in TIM-4+ B cells (**Supplementary Fig 5B**). Examination of these same cytokines reveals reduced frequency of expression in TIM-4+ B cells from *Rorc* KO mice, indicating partial, but not complete, dependence.

The pattern of cytokine genes expressed by TIM-4$^+$ B cells closely resembles that of pathogenic Th17 cells (pTh17) [22-24]. Comparing gene expression by TIM-4$^+$ B cells to TIM-1$^+$ B cells, demonstrates that in addition to the cytokines pathognomonic for pTh17 cells like *Csf2* and *Il22*,

TIM-4$^+$ B cells exhibit increased expression of a number of other genes in the pTh17 signature that we previously identified by polarizing pTh17 cells with TGFβ3 and IL-6, compared to non-pTh17 cells polarized with TGFβ1 and IL-6 (**Supplementary Fig. 5C)** [23]. These include chemokines such as *Ccl3*, *Ccl4*, and *Ccl5*, as well as *Stat4*, and *Lgals3* (encoding Galectin 3). However, not all genes upregulated in that pTh17 signature were upregulated in TIM-4$^+$ B cells. For example, *Icos, Cxcl3, Gzmb, Casp1* (encoding caspase I, required for IL-1β maturation) and *Tbx21*, were either expressed at lower levels or were not statistically higher in TIM-4$^+$ B cells. Amongst genes downregulated in pTh17 cells, *Il10, Maf, and Ikzf3* (IKAROS family Zinc Finger 3) are also downregulated in TIM-4$^+$ B cells, while *Cd5l* was upregulated and *Ahr* expression was variable in TIM-4$^+$ B cells (**Supplementary Fig. 5D)**. Of genes identified in several other pTh17 signatures[24-29], only *Batf, Bhle40*, and *Cd44* were upregulated in TIM-4$^+$ B cells, but not *Il23r*, the canonical Notch signaling mediator *Rbpj, IL1rn*, *Gpr65, Toso, Plzp, Batf3, Cd44, Prdm1*, Protein receptor C (*PROCR*), *Foxo1*, or IRF4, (**Supplementary Fig. 5C**). These data suggest that while expressing similar cytokines, the regulation of TIM-4$^+$ B cell induction and/or differentiation may be distinct from that of pTh17 cells.

DISCUSSION

In addition to antibody production, B cells play an important role enhancing or inhibiting immune responses through antigen presentation, the elaboration of cytokines and expression of coinhibitory and costimulatory ligands [1,2,4-6]. Despite the strong influence of various B cell-derived proinflammatory cytokines on anti-microbial, tumor, allo-, and auto- immunity, no broad marker for Beffs has been previously identified. Herein, we demonstrated that TIM-4 identifies proinflammatory Beff cells that selectively express RORγt, IL-17A, and additional proinflammatory cytokines resembling those expressed by pTh17 cells. Production of IL-17A by TIM-4$^+$ B cells is dependent on IL-23, RORγt, and IL-17 itself, which is required as a B cell autocrine factor. In the

absence of these underlying pro-inflammatory signals, TIM-4$^+$ B cells are dysregulated and now produce IL-10 and exhibit potent regulatory activity.

Until recently, our understanding of Breg biology was hampered by the lack a unifying marker. We have since shown that TIM-1 is a broad marker for Bregs, and regulates the expression of an array of anti-inflammatory cytokines and coinhibitory molecules[7,8]. Its specific deletion in B cells results in spontaneous systemic autoimmunity, including an EAE-like paralytic neuroinflammatory disorder[7]. In contrast, B cells can also produce a variety of proinflammatory cytokines that play important roles in inflammatory immune responses. These include: B cell production of TNFα and IL-2 (required for the clearance of *H. polygyrus*); IL-6 (augments EAE severity); GM-CSF (pathogenic role in EAE and multiple sclerosis); and IFNγ (requisite role in proteoglycan-induced arthritis, and determines the relative size of the germinal center versus extrafollicular response during infection) [2,5,6,12,30]. Yet, few studies have examined the phenotype of B cells producing any of these proinflammatory cytokines. We previously showed that TIM-4$^+$ B cells were proinflammatory, enhancing both tumor and allograft rejection[9]. This was initially attributed to their increased expression of IFNγ. We now show that TIM-4 identifies B cells that also express IL-17A, IL-17F, IL-22, IL-6, IL-1β, and GM-CSF. Thus, TIM-4$^+$ is a broad marker for B cells that express many of the proinflammatory cytokines previously attributed to B cell effector function. This allows us to begin to address how proinflammatory cytokine production is regulated in TIM-4$^+$ Beffs and differs from the signals regulating TIM-1$^+$ Breg activity.

Bermejo et al previously reported that in the isolated setting of *T. cruzii* infection, a pathogen-specific transialidase alters CD45 glycosylation, and this induces B cell IL-17A expression that is RORγt-independent[13]. Whereas adoptive transfer of WT B cells into μMT mice enhanced clearance of T. cruzii, IL-17$^{-/-}$ B cells had no effect. We now demonstrate that B cell IL-17A expression is a much more generalized component of B cell function, expressed in response to

various types of immunization at a frequency similar to that of B cell-derived IL-10. In these settings, IL-17A is RORγt-dependent and predominantly expressed by TIM-4+ B cells. In mice lacking B cell-derived IL-17A or RORγt, TIM-4^{+} B cells are dysregulated and significantly upregulate IL-10 resulting in strong regulatory activity leading to decreased CD4 and CD8 proliferation, increased Tregs, decreased Th17 and Th1 responses, reduced EAE severity, and prolonged allograft survival. Conversion between B cells with regulatory versus pro-inflammatory activity has not been previously described.

Non-pathogenic Th17 (npTh17) cells express IL-10 along with IL-17A, and while not frankly suppressive, they play an essential role maintaining the integrity of the gut mucosal barrier [31,32]. In contrast, pTh17 cells express little IL-10, but express IL-17A in conjunction with a host of other pro-inflammatory cytokines including, for example, GM-CSF which plays an important inflammatory role in EAE [32,33]. The equilibrium between npTh17 and pTh17 cells is carefully regulated by balancing IL-10 and IL-23R expression, respectively. For example, npTh17 cells express increased Cd5L, which interacts with fatty acid synthase to alter the lipid biosynthesis and reduce RORγt-agonistic ligands [21]. This reduces RORγt-DNA binding, resulting in decreased activation of the *Il23r* locus and reduced repression of the *Il10* locus, which together, favor the differentiation of npTh17 rather than pTh17 cells. In contrast, increased RBPJ, a mediator of NOTCH signaling, enhances *Il23r* expression which drives pTh17 differentiation [34].

IL-23 is also an important driver of the TIM-4^{+} pro-inflammatory module which shares many similarities to that of pTh17 cells including cytokines, chemokines (*Ccl3, Ccl4, Ccl5), Lgals3* (encoding Galectin3), and *Stat4* [23]. Despite this resemblance, the regulation of proinflammatory cytokine versus IL-10 expression by TIM-4^{+} B cells, and between TIM-4^{+} Beffs and the opposing TIM-1^{+} Breg subset, differs from that in npTh17 and pTh17 cells. For example, compared to TIM-1^{+} Bregs, TIM-4^{+} B cells express increased *Cd5l,* which as noted above, is more highly expressed in npTh17 cells, where it promotes IL-10 and inhibits Il23r expression, thereby inhibiting

proinflammatory function. While TIM-4$^+$ B cells express little *Il10* and are proinflammatory, CD5L may act to modulate their proinflammatory activity. Moreover, neither *RBPJ* nor *Il23r* are differentially expressed, consistent with IL-23 responsiveness by both TIM-1 and TIM-4$^+$ B cells. Indeed, IL-23R signaling reduces IL-10 expression in both TIM-1$^+$ and TIM-4$^+$ B cells. Yet, IL-23 only induces inflammatory cytokine expression in TIM-4$^+$ B cells, likely due to their almost exclusive expression of RORγt. In addition to its requisite role in IL-17A expression, RORγt augments the expression of other proinflammatory cytokines by TIM-4+ Beffs, as in pTh17 cells. In this regard, TIM-4$^+$ B cells differentially express *Bhle40*, a basic helix-loop-helix transcription factor that promotes *Csf2* and inhibits *Il10* expression in pTh17 cells, and *BatF*, an AP-1 transcription factor that transactivates *Il17* and *Il22* expression [35,36]. Thus, TIM-1$^+$ and TIM-4$^+$ B cells with opposing functions as Beffs and Bregs, respectively, exhibit distinct signals that differentially regulate regulatory and proinflammatory cytokine loci.

We showed that exogenous IL-17A directly inhibits IL-10 production by TIM-4$^+$ B cells *in vitro*. IL-23 also inhibits IL-10 production by TIM-4+ B cells, including those from RORγt iBKO mice, indicating an IL-17-independent effect. However, in WT TIM-4+ B cells, IL-10 expression in enhanced by neutralizing IL-17, despite exogenous IL-23 and intact (endogenous) RORgt, suggesting that IL-17 plays a dominant role. This is supported by BM chimeric mice with a B cell-specific deletion of *Il17a* which exhibit significantly increased IL-10 production by B cells - also indicating that IL-17 plays an autocrine role inhibiting B cell IL-10 production *in vivo*. This suggests that TIM+4+ B cells largely reside near other B cells and away from other endogenous sources of IL-17. To our knowledge, a pathway leading from IL-17A signaling to IL-10 inhibition has not been previously described and will require further study. This IL-17 pathway does not predominate in TIM-1$^+$ B cells where IL-23 signals strongly inhibit IL-10 despite barely detectable IL-17A expression, and only modest recovery of IL-10 expression occurs upon IL-17A neutralization. Addition of exogenous IL-17 does not suppress IL-10 expression by TIM-1$^+$ B cells beyond that

seen with IL-23 alone. However, in the absence of IL-23/IL-23R signaling, exogenous IL-17 does inhibit *Il10* expression by TIM-1$^+$ B cells, indicating that IL-17 and IL-23 independently inhibit *Il10* expression. Finally, we showed that RORγt plays an IL-17 and IL-23 independent role on the inhibition of IL-10 expression in TIM-4+ B cells. This is consistent with our previous findings that RORγt can bind to the IL-10 promotor and inhibit its expression [21].

In summary, in TIM-4$^+$ B cells, IL-23 drives the expression of a proinflammatory module which includes RORγt-dependent IL-17A production. IL-17A acts in an autocrine manner to enhance its own expression, and along with RORγt, suppresses IL-10 and enforces pro-inflammatory Beff activity. In contrast, IL-23 has minimal effect on proinflammatory cytokine expression by TIM-1$^+$ B cells which lack RORγt, while IL-23 and IL-17A independently inhibit IL-10 expression. These findings suggest that cross-regulation may occur at several levels. IL-23 in the microenvironment should inhibit *Il10* expression by TIM-1$^+$ B cells and augment expression of the TIM-4$^+$ proinflammatory module. IL-17A expressed by TIM-4$^+$ B cells not only enforces their Beff activity but may suppress *Il10* expression by TIM-1$^+$ Bregs. Finally, impaired IL-17 production by TIM-4$^+$ Beffs results in their increased *Il1*0 expression and Breg activity. Thus, we have identified a reciprocal relationship between B cells with regulatory and effector activity. In this regard, we recently showed that deletion of TIM-1 expression in B cells inhibits tumor progression and results in the expansion of B cells in the draining LNs that express proinflammatory cytokines in a type I IFN-mediated manner[37]. Whether this is due to the acquisition of inflammatory function by B cells that were destined to become TIM-1$^+$ Bregs, or due to increased TIM-4$^+$ Beffs in the absence of TIM-1$^+$ Bregs, is not yet clear. In conclusion, TIM-4 is a broad marker for RORgt-expressing B cells that exhibit Beff function. IL-23 and IL-17A selectively enhance proinflammatory cytokine expression by TIM-4+ B cells, while preventing their conversion into IL-10-expressing B cells with regulatory activity. Further elucidation of these signals may allow therapeutic manipulation of TIM-

4+ B cells to appropriately inhibit or enhance the immune response in settings of autoimmunity, transplantation, and cancer.

METHODS:

Study Design: To further study the role of TIM-4+ B cells, we examined their cytokine production by flow cytometry and confirmed results using IL-17-reporter mice, and in vitro cytokine secretion. The role of B cell IL-17 was studied in EAE and islet allograft models by B cell adoptive transfer, generation of BM chimeras, and inducible B cell specific RORγt knockouts. These studies revealed an inverse relationship between IL-17 and IL-10 expression. The role of various cytokines in regulating IL-17 vs. IL-10 expression was directly tested in Tim-4+ as well as Tim-1+ Bregs in vitro by RT-PCR and cytokine secretion assays. Finally, Bulk RNAseq was performed to reveal that Tim-4+ Beffs express a module of proinflammatory cytokines, allowing a comparison to the genes signature of pTh17 cells. Previously published methods and those not used in the main Figs. are described in Supplementary Methods.

Mice: C57BL/6 (B6; H-2b), BALB/c (H-2d), *Rorc*$^{-/-}$, *Rorc*$^{fl/fl}$, *Il17a*$^{-/-}$, B6 IL-17A–EGFP reporter, OT-I transgenic, OT-II transgenic and μMT (B6) mice were from The Jackson Laboratory. *hCd20-ERT2.Cre* (from Mark Shlomchik, University of Pittsburgh[38] were crossed with Rorc$^{fl/fl}$ mice to generate *Rorc*$^{fl/fl}$*.hCd20Cre*$^{+/-}$ (RORγt iBKO) mice. Act-mOVA F1 mice (from Fadi Lakkis, University of Pittsburgh) were generated by breeding BALB/c with B6.*Act-OVA* mice[19]. Mice were used at 6–10 weeks of age and were housed with food and water ad libitum.

Islet transplantation and alloantigen immunization: 400 allogeneic islets from BALB/c donors were transplanted under the left renal capsule of sex-matched B6 recipients with streptozotocin-induced diabetes, as previously described [8,9]. In some experiments, mice were alloimmunized by i.p. injection of 2×10^7 mitomycin C–treated BALB/c splenocytes[8,9].

Flow cytometry: Fluorochrome-conjugated mAbs were purchased from BD Biosciences, eBioscience, and BioLegend. Staining was performed in the presence of Fc block(anti-CD16/CD32) and LIVE/DEAD Fixable Aqua viability indicator as described [8,9]. Flow acquisition

was performed on LSRII analyzers (BD Biosciences), and data were analyzed using FlowJo software (BD). Background staining was determined with isotype-matched controls or GFP^- littermates. Detection of intracellular cytokine detection by flow cytometry was previously described [8,9]. Briefly, T cells were cultured 4 h with PMA (50 ng/ml), ionomycin (500 ng/ml), and GolgiPlug (1 µl/ml). For IL-10, B cells were cultured 5 hours with LPIM (LPS (10 µg/ml), PMA, ionomycin, and monensin (1 µl/ml)). For IL-17, and other proinflammtory cytokines, B cells were cultured 5 hours with PIB (PMA, ionomycin, and Brefeldin A (1 µl/ml)). Cells were permeabilized using intracellular staining kits from BD Biosciences or eBioscience.

Cell preparation and adoptive transfer: B cells were isolated from spleens of naïve or alloimmunized (d14) WT or $IL17^{-/-}$ mice by negative selection (EasySep; StemCell Technologies; purity >98%). $CD19^+TIM\text{-}4^+$ and $CD19^+$ $TIM\text{-}4^-$ B cells were subsequently isolated by FACS using BD FACSAria (>95% purity). 5–7 $\times 10^6$ purified B cell subsets from naïve or alloimmunized syngeneic mice were adoptively transferred (i.v.) into otherwise untreated µMT recipients followed by islet transplants or EAE induction.

EAE: Mice were immunized s.c. with MOG 35–55 (200µg) and CFA (200 µl; Difco Laboratories) and received pertussis toxin (200 ng/mouse; ip) on days 0 and 2 [7]. Mice were scored daily for severity of EAE, as described [7].

Bone marrow (BM) chimeric mice: µMT (H-2b) mice were lethally irradiated (1000 rad) and reconstituted with 80:20 mixtures of syngeneic BM cells from: µMT plus WT, µMT plus *Il17a*$^{-/-}$, or µMT plus *Rorc*$^{-/-}$ donors [9]. BM chimeras were used after 8 weeks to allow immune reconstitution. B cells were fully reconstituted (from non-µMT BM).

Cytokine Secretion: IL-17A and IL-10 concentration in supernatants of B cells/subsets after 48 hours of stimulation with anti-IgM plus various cytokine. PMA and ionomyicn were added for the final 5h. was determined by Mouse Cytokine Cytometric Bead Array (CBA) and associated

software per manufacturer's instructions (BD Biosciences). 3000 events were acquired per sample on an LSR II (BD) analyzer.

RNA isolation, real-time PCR: *Splenic CD19+ B cells, isolated from alloimmunized B6 mice using the EasySep™ Mouse Pan-B Cell Isolation Kit (STEMCELL; purity >98%), were subsequently sorted based on staining criteria as CD19+ TIM-1+TIM-4-, TIM-4+TIM-1-, and DN (DUMP-negative for CD3, CD64, Gr-1, Ter119) populations. These sorted B cells were then stimulated with anti-IgM along with various cytokines for 24 hours, with the addition of PMA and ionomycin during the final 3 hours of stimulation.* Total RNA was extracted using RNeasy Micro Kit (Qiagen). 100ng of total RNA was used for cDNA synthesis by RNA to cDNA EcoDry™ Premix (Double Primed) kit (Takara), and qPCR was performed using Taqman primers with TaqMan™ Fast Advanced Master Mix on StepOnePlus Real-Time PCR Systems (Applied Biosystems). Relative expression was calculated using the ΔΔCt method and level was normalized to *GAPDH*. Taqman primers and probes were from Applied Biosystems: Mm00439618_m1 (*IL-17A*), Mm01288386_m1(IL-10), Hs02786624_g1(GAPDH).

RNA-seq: B cells were purified and stimulated as above except sorting was repeated 2-3X until the purity was ~100%. Total RNA quality was checked using a Bioanalyzer-2100 (Agilent Technologies) and submitted to the University of Pittsburgh Health Sciences Sequencing Core. Libraries were prepared (Ultra-low input RNA-seq Preparation Kit; Takara) and subjected to paired end sequencing (2 × 75 bp) using Illumina/NextSeq. Data was returned as NextSeq Fastq files.

Analysis of bulk RNA-seq data: Bulk RNA-seq data were preprocessed on the Google Cloud Platform via the Terra scientific computing platform (Terra.Bio). Briefly, raw reads were aligned to the mouse genome mm10 using the STAR (v2.7.5a) alignment tool. Duplicate reads were identified using Picard MarkDuplicates. RNA-SeQC 2 was used for assessing sequencing depth and mapping

quality. Raw counts and transcript per million (TPM) estimates were quantified using RSEM. All samples passed quality control and were included in subsequent analyses.

Downstream analyses were carried out in R (v4.1.3). Principal Component Analysis (PCA) was conducted using the R function *prcomp*. The gene with the highest PC2 loading, AY036118, was removed since it represents ribosomal RNA contamination[39]. Differential gene expression analysis was performed using DESeq2 (v1.32.0). Lowly expressed genes with a total count lower than 10 were prefiltered. P-values were adjusted by Benjamini-Hochberg (BH) method[40], and log2 fold changes were shrunk using the 'apeglm' algorithm[41]. Shrunken fold changes are depicted in all Figs. Heatmaps were created using R package ComplexHeatmap (v2.13.1) on normalized counts (normalized using the *counts* function from the BiocGenerics package (v0.40.0)[42] and were scaled by row. Volcano plots were generated using ggplot2 (v3.4.2) and ggrepel (v0.9.3).

Statistics. Statistical analyses of allograft survival used log-rank (Mantel-Cox) test. Differences were considered to be significant at *P* values <0.05. The clinical score and incidence of EAE were analyzed by 2-way Anova, and comparisons for results (mean ± SEM) for cytometric bead array. FACS, and real-time PCR were analyzed by Student's 2-tailed *t* test with p <0.05 considered significant. Paired 2-tailed t-test was used when cells from the same mouse were compared. Significantly differentially expressed genes for RNA-seq analysis were identified using DESeq2 with Benjamini-Hochberg adjusted p-value <0.05. No statistical methods were used to predetermine sample sizes, but our sample sizes are standard for the field[7,8]. No data were excluded unless stated otherwise. Data distribution was assumed to be normal, but this was not formally tested.

Reporting summary: Further information on research design is available in the Nature Portfolio Reporting Summary linked to this article.

Study approval: Animal studies were approved by the Institutional Animal Care and Use Committee at the University of Pittsburgh (Pittsburgh, PA, USA).

Data availability: All bulk RNA-seq data have been deposited in the NCBI's Gene Expression Omnibus (GEO) database and are publicly available under accession number: GSE253925. All raw data and materials will be made available to investigators upon request.

Acknowledgements: We would like to thank Dr. Mark Shlomchik for supplying the hCD20.ERT2.Cre mice. Funding: This research was supported by PO1 AI129880.

Author contributions: QD and DMR conceived the project. QD designed and performed most biological experiments. DMR supervised the study with key input from VKK. JLG provided data. ET and YW performed, and AS supervised, computational analysis. QD and DMR analyzed the data. QD, JLG, VKK, and DMR wrote the paper with input from all the authors.

References:

1. Mauri, C., and Menon, M. (2015). The expanding family of regulatory B cells. International immunology *27*, 479-486. 10.1093/intimm/dxv038.
2. Cherukuri, A., Ding, Q., Sharma, A., Mohib, K., and Rothstein, D.M. (2019). Regulatory and Effector B Cells: A New Path Toward Biomarkers and Therapeutic Targets to Improve Transplant Outcomes? Clin Lab Med *39*, 15-29. 10.1016/j.cll.2018.10.011.
3. Cherukuri, A., Mohib, K., and Rothstein, D.M. (2021). Regulatory B cells: TIM-1, transplant tolerance, and rejection. Immunol Rev *299*, 31-44. 10.1111/imr.12933.
4. Lund, F.E., and Randall, T.D. (2010). Effector and regulatory B cells: modulators of CD4+ T cell immunity. Nature reviews. Immunology *10*, 236-247. 10.1038/nri2729.
5. Lino, A.C., Dorner, T., Bar-Or, A., and Fillatreau, S. (2016). Cytokine-producing B cells: a translational view on their roles in human and mouse autoimmune diseases. Immunological reviews *269*, 130-144. 10.1111/imr.12374.
6. Fillatreau, S. (2015). Pathogenic functions of B cells in autoimmune diseases: IFN-gamma production joins the criminal gang. European journal of immunology *45*, 966-970. 10.1002/eji.201545544.
7. Xiao, S., Bod, L., Pochet, N., Kota, S.B., Hu, D., Madi, A., Kilpatrick, J., Shi, J., Ho, A., Zhang, H., et al. (2020). Checkpoint Receptor TIGIT Expressed on Tim-1(+) B Cells Regulates Tissue Inflammation. Cell Rep *32*, 107892. 10.1016/j.celrep.2020.107892.
8. Ding, Q., Yeung, M., Camirand, G., Zeng, Q., Akiba, H., Yagita, H., Chalasani, G., Sayegh, M.H., Najafian, N., and Rothstein, D.M. (2011). Regulatory B cells are identified by expression of TIM-1 and can be induced through TIM-1 ligation to promote tolerance in mice. The Journal of clinical investigation *121*, 3645-3656. 10.1172/JCI46274.
9. Ding, Q., Mohib, K., Kuchroo, V., and Rothstein, D. (2017). TIM-4 Identifies IFN-gamma-Expressing Proinflammatory B Effector 1 Cells That Promote Tumor and Allograft Rejection. Journal of immunology *199*, 2585-2595.
10. Wojciechowski, W., Harris, D.P., Sprague, F., Mousseau, B., Makris, M., Kusser, K., Honjo, T., Mohrs, K., Mohrs, M., Randall, T., and Lund, F.E. (2009). Cytokine-producing effector B cells regulate type 2 immunity to H. polygyrus. Immunity *30*, 421-433. 10.1016/j.immuni.2009.01.006.
11. Barr, T.A., Shen, P., Brown, S., Lampropoulou, V., Roch, T., Lawrie, S., Fan, B., O'Connor, R.A., Anderton, S.M., Bar-Or, A., et al. (2012). B cell depletion therapy ameliorates autoimmune disease through ablation of IL-6-producing B cells. The Journal of experimental medicine *209*, 1001-1010. 10.1084/jem.20111675.
12. Olalekan, S.A., Cao, Y., Hamel, K.M., and Finnegan, A. (2015). B cells expressing IFN-gamma suppress Treg-cell differentiation and promote autoimmune experimental arthritis. European journal of immunology *45*, 988-998. 10.1002/eji.201445036.
13. Bermejo, D.A., Jackson, S.W., Gorosito-Serran, M., Acosta-Rodriguez, E.V., Amezcua-Vesely, M.C., Sather, B.D., Singh, A.K., Khim, S., Mucci, J., Liggitt, D., et al. (2013). Trypanosoma cruzi trans-sialidase initiates a program independent of the transcription factors RORgammat and Ahr that leads to IL-17 production by activated B cells. Nature immunology *14*, 514-522. 10.1038/ni.2569.

14. Bar-Or, A., Fawaz, L., Fan, B., Darlington, P.J., Rieger, A., Ghorayeb, C., Calabresi, P.A., Waubant, E., Hauser, S.L., Zhang, J., and Smith, C.H. (2010). Abnormal B-cell cytokine responses a trigger of T-cell-mediated disease in MS? Ann Neurol *67*, 452-461. 10.1002/ana.21939.
15. Li, R., Rezk, A., Miyazaki, Y., Hilgenberg, E., Touil, H., Shen, P., Moore, C.S., Michel, L., Althekair, F., Rajasekharan, S., et al. (2015). Proinflammatory GM-CSF-producing B cells in multiple sclerosis and B cell depletion therapy. Sci Transl Med *7*, 310ra166. 10.1126/scitranslmed.aab4176.
16. Fillatreau, S., Sweenie, C.H., McGeachy, M.J., Gray, D., and Anderton, S.M. (2002). B cells regulate autoimmunity by provision of IL-10. Nat Immunol *3*, 944-950. 10.1038/ni833 ni833 [pii].
17. Zhao, D., Abou-Daya, K.I., Dai, H., Oberbarnscheidt, M.H., Li, X.C., and Lakkis, F.G. (2020). Innate Allorecognition and Memory in Transplantation. Front Immunol *11*, 918. 10.3389/fimmu.2020.00918.
18. Suchin, E.J., Langmuir, P.B., Palmer, E., Sayegh, M.H., Wells, A.D., and Turka, L.A. (2001). Quantifying the frequency of alloreactive T cells in vivo: new answers to an old question. Journal of immunology *166*, 973-981. 10.4049/jimmunol.166.2.973.
19. Abou-Daya, K.I., Tieu, R., Zhao, D., Rammal, R., Sacirbegovic, F., Williams, A.L., Shlomchik, W.D., Oberbarnscheidt, M.H., and Lakkis, F.G. (2021). Resident memory T cells form during persistent antigen exposure leading to allograft rejection. Sci Immunol *6*. 10.1126/sciimmunol.abc8122.
20. Mohib, K., Cherukuri, A., Yu, Z., Ding, Q., Watkins, S., and Rothstein, D. (2020). Antigen-dependent interactions between regulatory B cells and T cells at the T:B border inhibit subsequent T cell interactions with DCs. Am J Transplant *20*, 52-63.
21. Wang, C., Yosef, N., Gaublomme, J., Wu, C., Lee, Y., Clish, C.B., Kaminski, J., Xiao, S., Meyer Zu Horste, G., Pawlak, M., et al. (2015). CD5L/AIM Regulates Lipid Biosynthesis and Restrains Th17 Cell Pathogenicity. Cell *163*, 1413-1427. 10.1016/j.cell.2015.10.068.
22. Bettelli, E., Carrier, Y., Gao, W., Korn, T., Strom, T.B., Oukka, M., Weiner, H.L., and Kuchroo, V.K. (2006). Reciprocal developmental pathways for the generation of pathogenic effector TH17 and regulatory T cells. Nature *441*, 235-238. 10.1038/nature04753.
23. Lee, Y., Awasthi, A., Yosef, N., Quintana, F.J., Xiao, S., Peters, A., Wu, C., Kleinewietfeld, M., Kunder, S., Hafler, D.A., et al. (2012). Induction and molecular signature of pathogenic TH17 cells. Nat Immunol *13*, 991-999. 10.1038/ni.2416.
24. Langrish, C.L., Chen, Y., Blumenschein, W.M., Mattson, J., Basham, B., Sedgwick, J.D., McClanahan, T., Kastelein, R.A., and Cua, D.J. (2005). IL-23 drives a pathogenic T cell population that induces autoimmune inflammation. The Journal of experimental medicine *201*, 233-240. 10.1084/jem.20041257.
25. Thakore, P., Schnell, A., Zhao, M., Huang, L., Hou, Y., Christian, E., Zaghouani, S., Wang, C., Singh, V., Ma, S., et al. (2022). The chromatin landscape of Th17 cells reveals mechanisms of diversification of regulatory and pro-inflammatory states. bioRxiv 2022.02.26.482041; . https://doi.org/10.1101/2022.02.26.482041.
26. Yoo, S.A., Kim, M., Kang, M.C., Kong, J.S., Kim, K.M., Lee, S., Hong, B.K., Jeong, G.H., Lee, J., Shin, M.G., et al. (2019). Placental growth factor regulates the generation of T(H)17

cells to link angiogenesis with autoimmunity. Nat Immunol *20*, 1348-1359. 10.1038/s41590-019-0456-4.

27. Shimada, K., Porritt, R.A., Markman, J.L., O'Rourke, J.G., Wakita, D., Noval Rivas, M., Ogawa, C., Kozhaya, L., Martins, G.A., Unutmaz, D., et al. (2018). T-Cell-Intrinsic Receptor Interacting Protein 2 Regulates Pathogenic T Helper 17 Cell Differentiation. Immunity *49*, 873-885 e877. 10.1016/j.immuni.2018.08.022.
28. Wu, B., Zhang, S., Guo, Z., Wang, G., Zhang, G., Xie, L., Lou, J., Chen, X., Wu, D., Bergmeier, W., et al. (2018). RAS P21 Protein Activator 3 (RASA3) Specifically Promotes Pathogenic T Helper 17 Cell Generation by Repressing T-Helper-2-Cell-Biased Programs. Immunity *49*, 886-898 e885. 10.1016/j.immuni.2018.09.004.
29. Gaublomme, J.T., Yosef, N., Lee, Y., Gertner, R.S., Yang, L.V., Wu, C., Pandolfi, P.P., Mak, T., Satija, R., Shalek, A.K., et al. (2015). Single-Cell Genomics Unveils Critical Regulators of Th17 Cell Pathogenicity. Cell *163*, 1400-1412. 10.1016/j.cell.2015.11.009.
30. Elsner, R.A., Smita, S., and Shlomchik, M.J. (2024). IL-12 induces a B cell-intrinsic IL-12/IFNγ feed-forward loop promoting extrafollicular B cell responses. Nat Immunol *25*, 1283-1295. 10.1038/s41590-024-01858-1.
31. Stockinger, B., and Omenetti, S. (2017). The dichotomous nature of T helper 17 cells. Nature reviews. Immunology *17*, 535-544. 10.1038/nri.2017.50.
32. Pawlak, M., Ho, A.W., and Kuchroo, V.K. (2020). Cytokines and transcription factors in the differentiation of CD4(+) T helper cell subsets and induction of tissue inflammation and autoimmunity. Current opinion in immunology *67*, 57-67. 10.1016/j.coi.2020.09.001.
33. Codarri, L., Gyulveszi, G., Tosevski, V., Hesske, L., Fontana, A., Magnenat, L., Suter, T., and Becher, B. (2011). RORgammat drives production of the cytokine GM-CSF in helper T cells, which is essential for the effector phase of autoimmune neuroinflammation. Nat Immunol *12*, 560-567. 10.1038/ni.2027.
34. Meyer Zu Horste, G., Wu, C., Wang, C., Cong, L., Pawlak, M., Lee, Y., Elyaman, W., Xiao, S., Regev, A., and Kuchroo, V.K. (2016). RBPJ Controls Development of Pathogenic Th17 Cells by Regulating IL-23 Receptor Expression. Cell Rep *16*, 392-404. 10.1016/j.celrep.2016.05.088.
35. Schraml, B.U., Hildner, K., Ise, W., Lee, W.L., Smith, W.A., Solomon, B., Sahota, G., Sim, J., Mukasa, R., Cemerski, S., et al. (2009). The AP-1 transcription factor Batf controls T(H)17 differentiation. Nature *460*, 405-409. 10.1038/nature08114.
36. Lin, C.C., Bradstreet, T.R., Schwarzkopf, E.A., Sim, J., Carrero, J.A., Chou, C., Cook, L.E., Egawa, T., Taneja, R., Murphy, T.L., et al. (2014). Bhlhe40 controls cytokine production by T cells and is essential for pathogenicity in autoimmune neuroinflammation. Nat Commun *5*, 3551. 10.1038/ncomms4551.
37. Bod, L., Kye, Y.-C., Shi, J., Triglia, E., Schnell, A., Fessler, J., Ostrowski, S., Von-Franque, M., Kuchroo, J., Barilla, R., et al. (2023). Single-cell profiling identifies B-cell specific checkpoint molecules that regulate antitumor immunity. Nature *619 348-356. doi: 10.1038/s41586-023-06231-0. Epub 2023 Jun 21. PMID: 37344597*, 348-356. 10.1038/s41586-023-06231-0.

38. Khalil, A.M., Cambier, J.C., and Shlomchik, M.J. (2012). B cell receptor signal transduction in the GC is short-circuited by high phosphatase activity. Science *336*, 1178-1181. 10.1126/science.1213368.
39. Akama-Garren, E.H., van den Broek, T., Simoni, L., Castrillon, C., van der Poel, C.E., and Carroll, M.C. (2021). Follicular T cells are clonally and transcriptionally distinct in B cell-driven mouse autoimmune disease. Nat Commun *12*, 6687. 10.1038/s41467-021-27035-8.
40. Benjamini, Y., and Hochberg, Y. (1995). Controlling the False Discovery Rate: A Practical and Powerful Approach to Multiple Testing. Journal of the Royal Statistical Society. Series B (Methodological) *57*, 289-300.
41. Zhu, A., Ibrahim, J.G., and Love, M.I. (2018). Heavy-tailed prior distributions for sequence count data: removing the noise and preserving large differences. Bioinformatics *35*, 2084-2092. 10.1093/bioinformatics/bty895.
42. Huber, W., Carey, V.J., Gentleman, R., Anders, S., Carlson, M., Carvalho, B.S., Bravo, H.C., Davis, S., Gatto, L., Girke, T., et al. (2015). Orchestrating high-throughput genomic analysis with Bioconductor. Nature Methods *12*, 115-121. 10.1038/nmeth.3252.

Figure 1

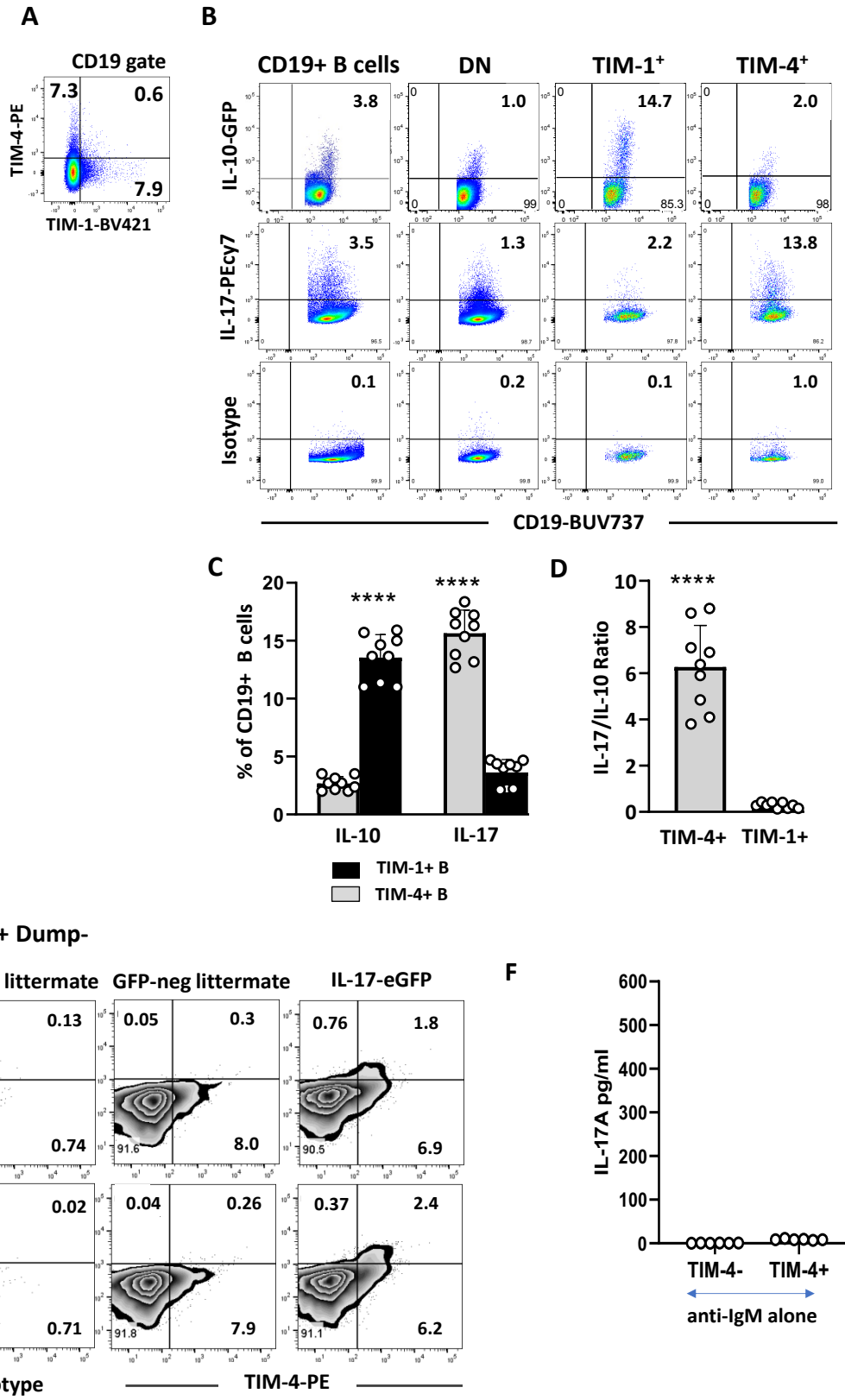
A
CD19 gate
TIM-4-PE
TIM-1-BV421
7.3
0.6
7.9
B
CD19+ B cells
DN
TIM-1+
TIM-4+
IL-10-GFP
IL-17-PEcy7
Isotype
3.8
1.0
14.7
2.0
3.5
1.3
2.2
13.8
0.1
0.2
0.1
1.0
CD19-BUV737
C
% of CD19+ B cells
****
****
IL-10
IL-17
TIM-1+ B
TIM-4+ B
D
IL-17/IL-10 Ratio
****
TIM-4+
TIM-1+
E
Gate: CD19+ Dump-
GFP-neg littermate
GFP-neg littermate
IL-17-eGFP
Unstim.
PIB 5hrs
IL-17-eGFP
0.13
0.13
0.74
0.05
0.3
8.0
0.76
1.8
6.9
0.11
0.02
0.71
0.04
0.26
7.9
0.37
2.4
6.2
isotype
TIM-4-PE
F
IL-17A pg/ml
****
TIM-4-
TIM-4+
TIM-4-
TIM-4+
anti-IgM alone
anti-IgM + IL-23

Fig 1. TIM-4$^+$ B cells are distinct from those expressing TIM-1$^+$ and preferentially express IL-17A. Splenic B cells from C57BL/6 mice 14 days after alloimmunization. (**A, B**) Representative flow cytometry plots: **(A)** TIM-1 and TIM-4 expression on CD19$^+$ B cells and **B**) IL-10 and IL-17A expression on total (CD19$^+$) B cells, TIM-1$^-$TIM-4$^-$ (DN), TIM-1$^+$, and TIM-4$^+$ B cell subpopulations. IL-17A isotype (control) shown in bottom row. (GFP-negative control for IL-10-GFP reporter not shown). (**C**) Bar graph showing mean frequency (+ SD) of IL-10 and IL-17A expression on TIM-1$^+$ vs. TIM-4$^+$ B cells based on flow cytometry, as in (**B**) (n=9 mice per group in 3 individual experiments). (**D**) Bar graph showing the ratio of IL-17A$^+$/IL-10$^+$ cells within TIM-1$^+$ and TIM-4$^+$ B cell subsets (mean + SD) based on data in (**C**). (**E**) Representative FACS plots showing TIM-4 and IL-17A-EGFP expression on unstimulated vs. PIB stimulated CD19$^+$ B cells from alloimmunized IL-17A-EGFP reporter mice. (n=3 mice per group). (**F**) IL-17 secretion by TIM-4$^+$ and TIM-4$^-$ CD19$^+$ B cells stimulated with anti-IgM +/- IL-23 for 48 hours (PMA/Ionomycin added for the final 5 hours). IL-17A concentration in the supernatants was measured by Cytometric Bead Array. (n=6 mice per group in 2 independent experiments). Statistics: * $p< 0.05$ vs. other groups; ** $p<0.01$ vs. other groups.

Figure 2

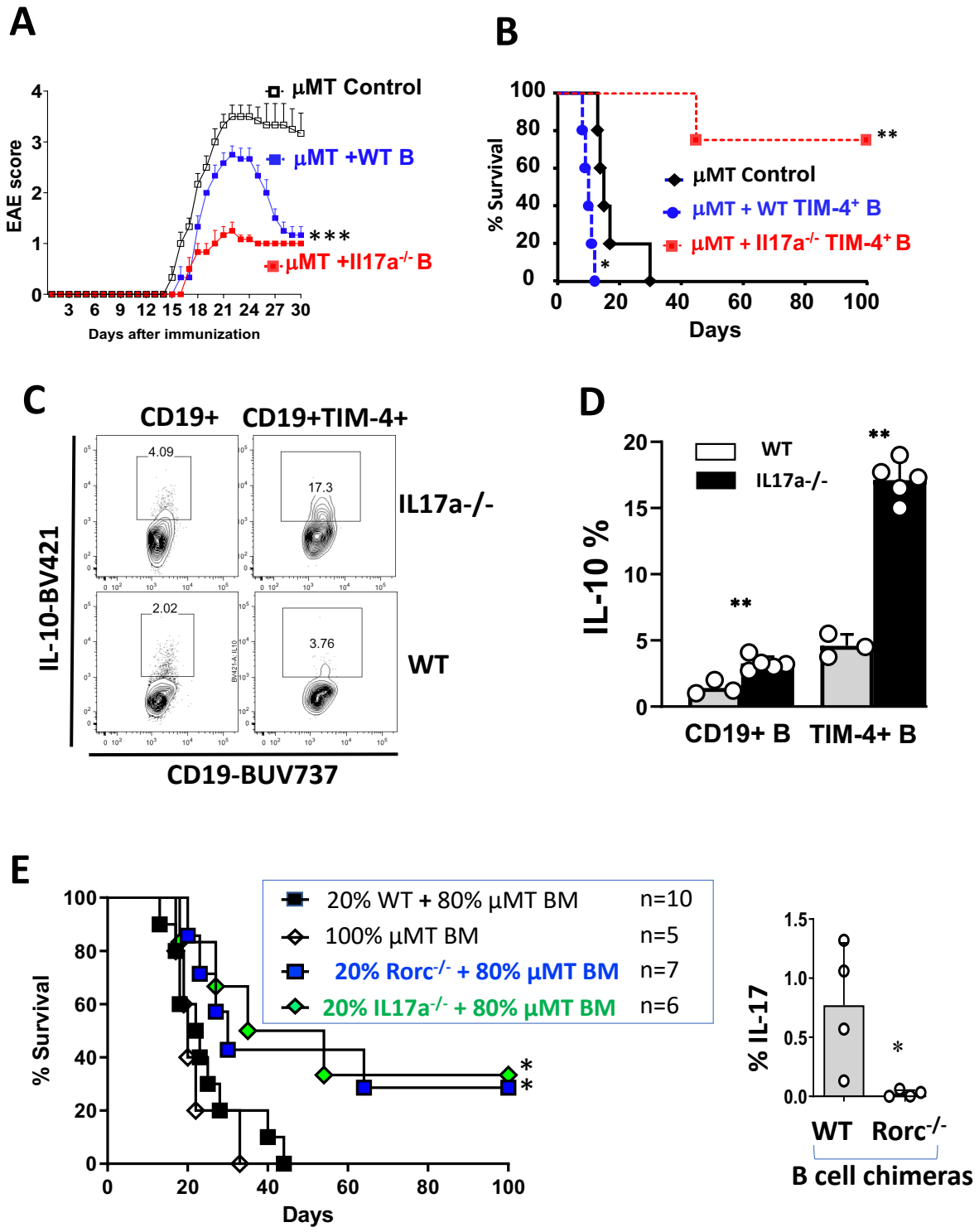
A
EAE score
Days after immunization
μMT Control
μMT +WT B
μMT +Il17a-/- B
***
B
% Survival
Days
μMT Control
μMT + WT TIM-4+ B
μMT + Il17a-/- TIM-4+ B
**
*
C
CD19+
CD19+TIM-4+
IL17a-/-
WT
4.09
17.3
2.02
3.76
IL-10-BV421
CD19-BUV737
D
IL-10 %
WT
IL17a-/-
**
**
CD19+ B
TIM-4+ B
E
% Survival
Days
20% WT + 80% μMT BM n=10
100% μMT BM n=5
20% Rorc-/- + 80% μMT BM n=7
20% IL17a-/- + 80% μMT BM n=6
*
*
% IL-17
*
WT
Rorc-/-
B cell chimeras

Figure 2 (cont)

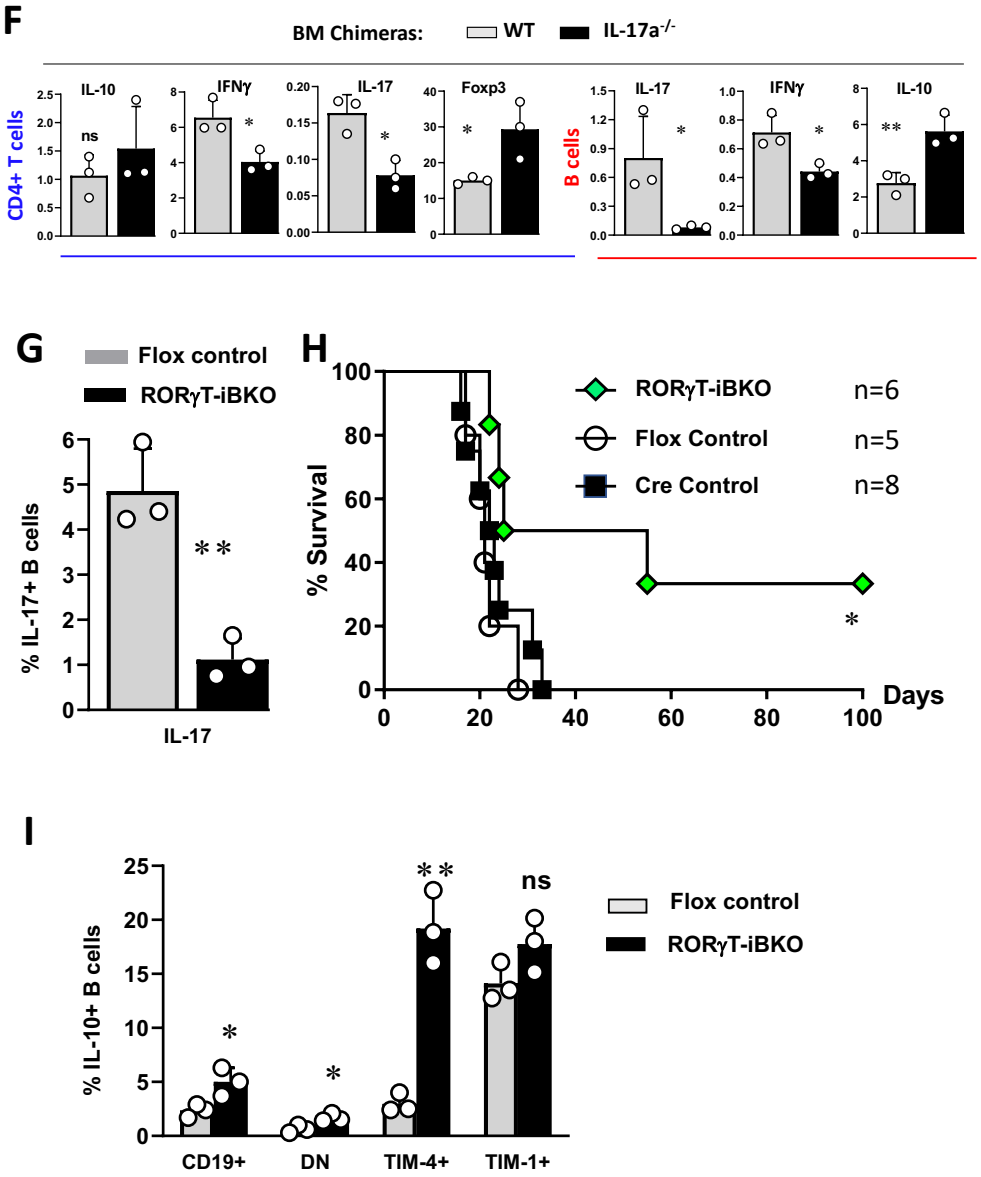

Fig 2. IL-17-deficient B cells are regulatory. (**A)** EAE was induced in μMT mice that received no B cells, or adoptive transfer of 10 $X10^6$ B cells from naive WT or IL-$17A^{-/-}$ mice. Fig. shows mean (+ SEM) EAE scores over time ($n \geq 6$ mice per group; representative of 2 independent experiments). ***$p < 0.001$ by 2-way ANOVA. (**B**) Kaplan–Meier plots showing survival of BALB/c islet allografts in diabetic μMT (B6) recipients that were untreated (control) or received 5×10^6 syngeneic TIM-4^+CD19^+ B cells from (day 14) alloimmunized WT or IL-$17^{-/-}$ donor mice. n=4-5 mice/group. *$p < 0.05$; **$p < 0.01$ versus control. (**C**) Representative flow cytometry plots of IL-10 expression by CD19^+ and TIM-4^+ B cells from alloimmunized IL-$17A^{-/-}$ versus WT B6 mice. **(D**) Bar graph showing mean frequency (+SD) of IL-10 expression on total (CD19^+) and TIM-4^+ B cells represented in panel (C). n = 3-5 mice/group. **$p < 0.01$. **(E)** μMT BM chimeric mice were reconstituted with 100% μMT BM or with 80% μMT BM plus 20% *Il17*$^{-/-}$, *Rorc*$^{-/-}$, or WT BM. **Left panel**: Kaplan-Meier plots showing BALB/c islet allograft survival in diabetic BM chimeric recipients (n=5-10 mice/group) *$p < 0.05$ vs. Controls. **Right panel**: Quantitation of IL-17A expression (intracellular staining) in alloimmunized WT vs. *Rorc*$^{-/-}$ BM chimeras (n=4 mice/group) *$p < 0.05$. **(F)** WT and *Il17a* BM chimeric mice were alloimmunized and cytokine (IL-10, IL-17, and IFN-γ) and Foxp3 expression on endogenous CD4^+ T cells and CD19^+ B cells was determined by intracellular flow cytometry. *$p<0.05$; **$p<0.01$. **(G)** Quantitation of frequency of IL-17^+ B cells in RORγt-iBKO vs. $Rorc^{fl/fl}$ (Flox Control) mice 14 days after alloimmunization. ** $p<0.01$. **(H)** Kaplan-Meier plots of BALB/c islet allograft survival in Tamoxifen-treated diabetic RORγt-iBKO versus Flox Control and hCD20.ERT2.$Cre^{+/-}$ (Cre control) recipients. n=5-8 mice/group *$p<0.05$. **(I)** Bar Graph showing mean frequency (mean + SD) of IL-10 expression on total B cells and B cell subpopulations (n=3 mice per group). *$p<0.05$, **$p < 0.01$ RORγt-iBKO vs. Flox Control mice.

Figure 3

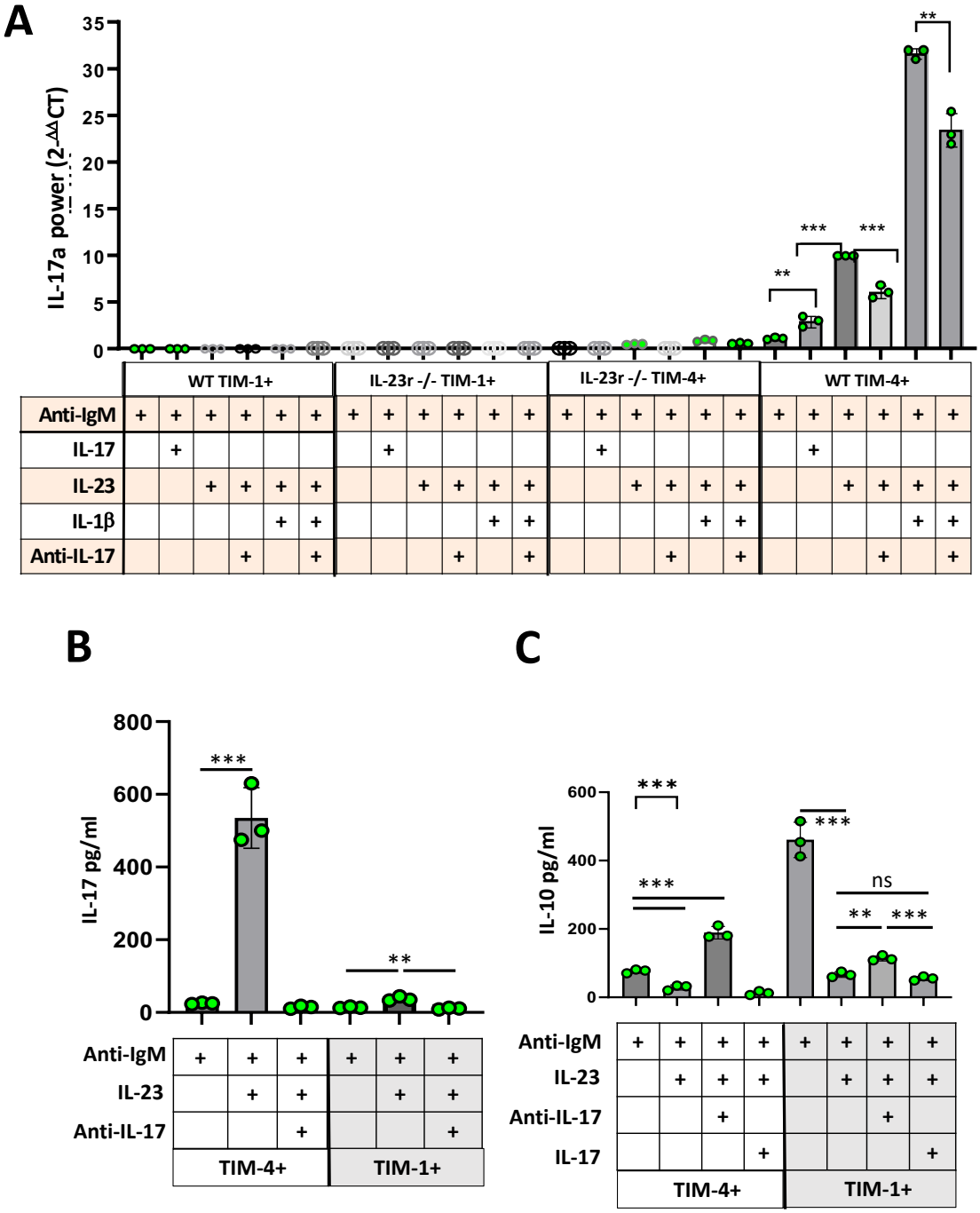
A
IL-17a power (2^-ΔΔCT)
35
30
25
20
15
10
5
0
**
***
***
**
WT TIM-1+
IL-23r -/- TIM-1+
IL-23r -/- TIM-4+
WT TIM-4+
Anti-IgM
IL-17
IL-23
IL-1β
Anti-IL-17
B
IL-17 pg/ml
800
600
400
200
0
***
**
Anti-IgM
IL-23
Anti-IL-17
TIM-4+
TIM-1+
C
IL-10 pg/ml
600
400
200
0
***
***
***
***
ns
**
***
Anti-IgM
IL-23
Anti-IL-17
IL-17
TIM-4+
TIM-1+

Figure 3

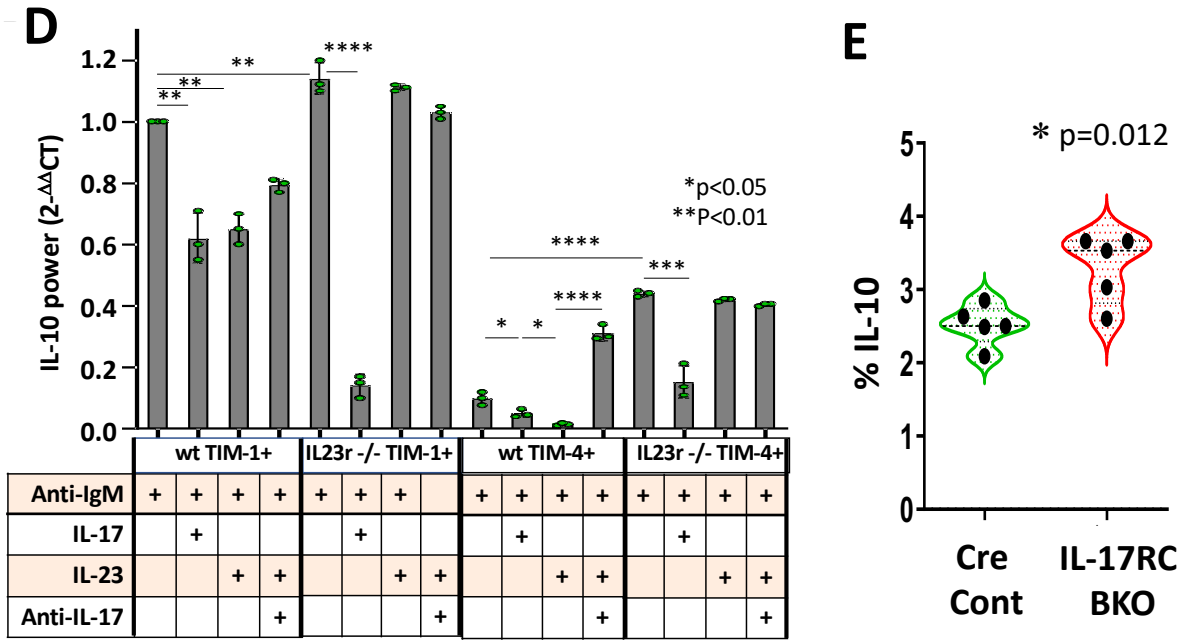

Fig 3. Regulation of IL-17A and IL-10 expression by IL-23 and IL-17.

(A) TIM-1^{+}TIM-4 and TIM-4^{+}TIM-1^{-} CD19^{+} B cells from alloimmunized *Il23r*$^{-/-}$ and WT B6 mice were stimulated for 24 hours with anti-IgM and cytokines or neutralizing anti-IL-17A as indicated. IL-17A expression was compared to that of GAPDH by qPCR. The bar graph shows the relative expression of IL-17A mRNA as 2-$^{\Delta\Delta}$CT performed in triplicate wells on cells pooled from 3 mice per group. **p<0.01; ***p<0.001. Data representative of three independent experiments.

(B-C) TIM-1^{+}TIM-4^{-} and TIM-4^{+}TIM-1^{-} B cells from alloimmunized WT B6 mice were stimulated with anti-IgM alone or anti-IgM plus IL-23, IL-17A or anti-IL-17A neutralizing antibody as indicated. Bar graphs display the concentration of IL-17A (**B**) and IL-10 (**C**) in the supernatants (performed in triplicate wells on cells pooled from 3 mice per group). Data representative of three independent experiments. **p<0.01 and ***p<0.001.

(D) TIM-1^{+}TIM-4^{-} and TIM-4^{+}TIM-1^{-}B cells from *Il23r*$^{-/-}$ and WT B6 mice, were stimulated and IL-10 mRNA expression assessed by qPCR as in (**A**) above. The bar graph shows the relative expression of IL-10 as 2-$^{\Delta\Delta}$CT in triplicate wells on cells pooled from 3 mice per group. **p<0.01; ***p<0.001. Data representative of three independent experiments. **(E)** Violin plot depicting mean frequency (+SD) of IL-10 expression (intracellular staining) on splenic CD19^{+} B cells from IL-17RC$^{fl/fl}$CD19-Cre$^{+/-}$ (IL-17RC-BKO) and CD19-Cre (Cre Control) mice. n=5 mice. *p<0.05.

Figure 4

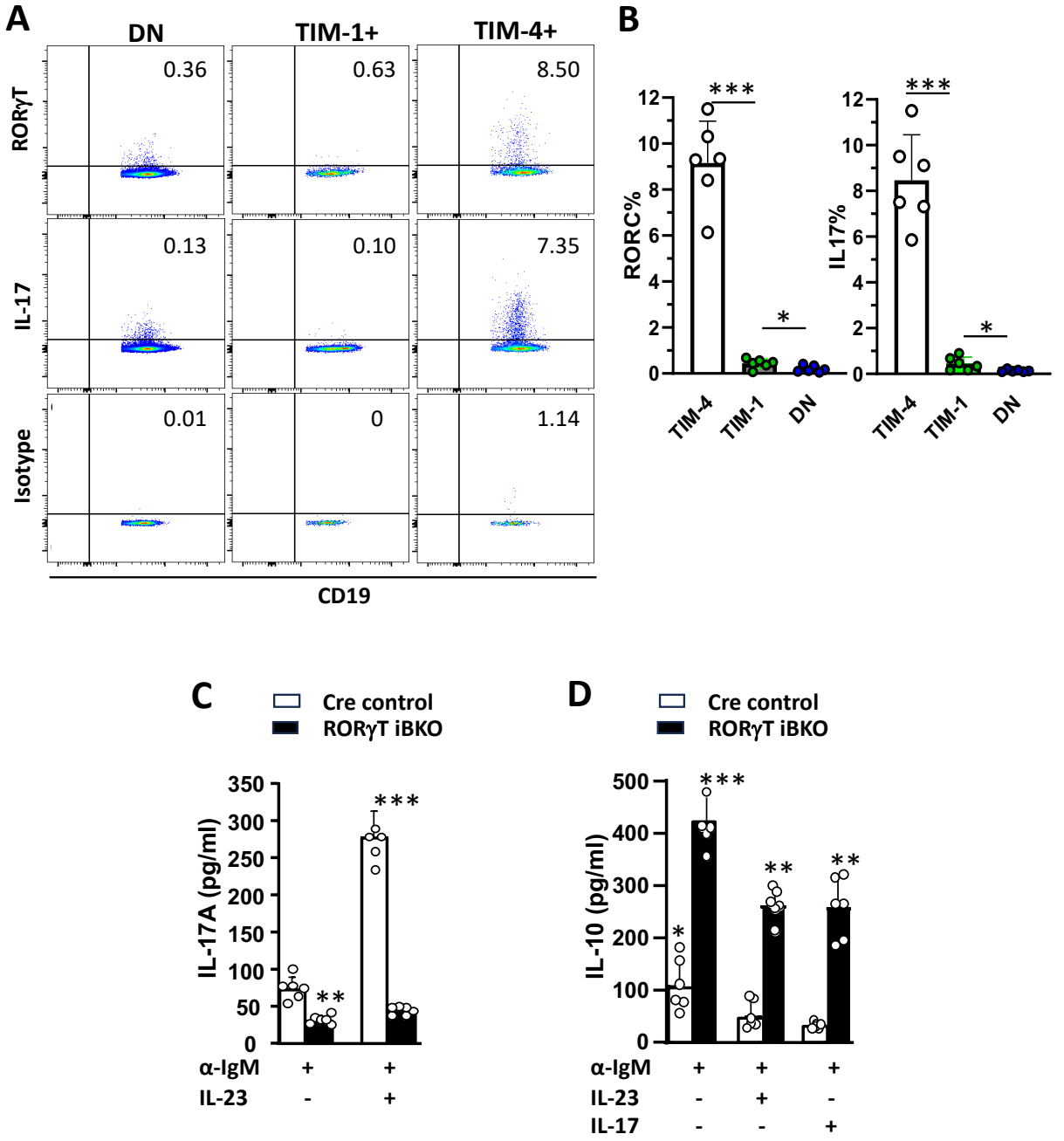

Figure 4 RORγt is selectively expressed by TIM-4+ B cells and this correlates directly with IL-17A expression. Splenic B cells from C57BL/6 mice 14 days after alloimmunization. (**A**) Representative flow cytometry plots show RORγT and IL-17A expression on total DN (TIM-1$^-$TIM-4$^-$), TIM-1$^+$, and TIM-4$^+$ B cell subpopulations. isotype (control) shown in bottom row. (**B**) Bar

graph showing mean frequency (+ SD) of RORγT and IL-17A expression on TIM-4$^+$, TIM-1$^+$ and DN B cells based on flow cytometry, as in (**A**). * $p < 0.05$; *** $p < 0.001$. (n=6 mice per group in 2 independent experiments). (**C, D**) Purified CD19+B cells from spleens of TAM-treated RORγT iBKO and Cre control mice were stimulated in vitro with anti-IgM alone plus IL-23, or IL-17A for 48 hours. Bar graphs display the concentration IL-17A (**C**) , and IL-10 (**D**) in the supernatants, as measured by Cytometric Bead Array. * $p <0.03$ vs. other Control groups; ** $p<0.001$ vs. corresponding Control group; ***$p<0.001$ vs. all other groups. (n=6 mice per group, in 2 independent experiments).

Figure 5

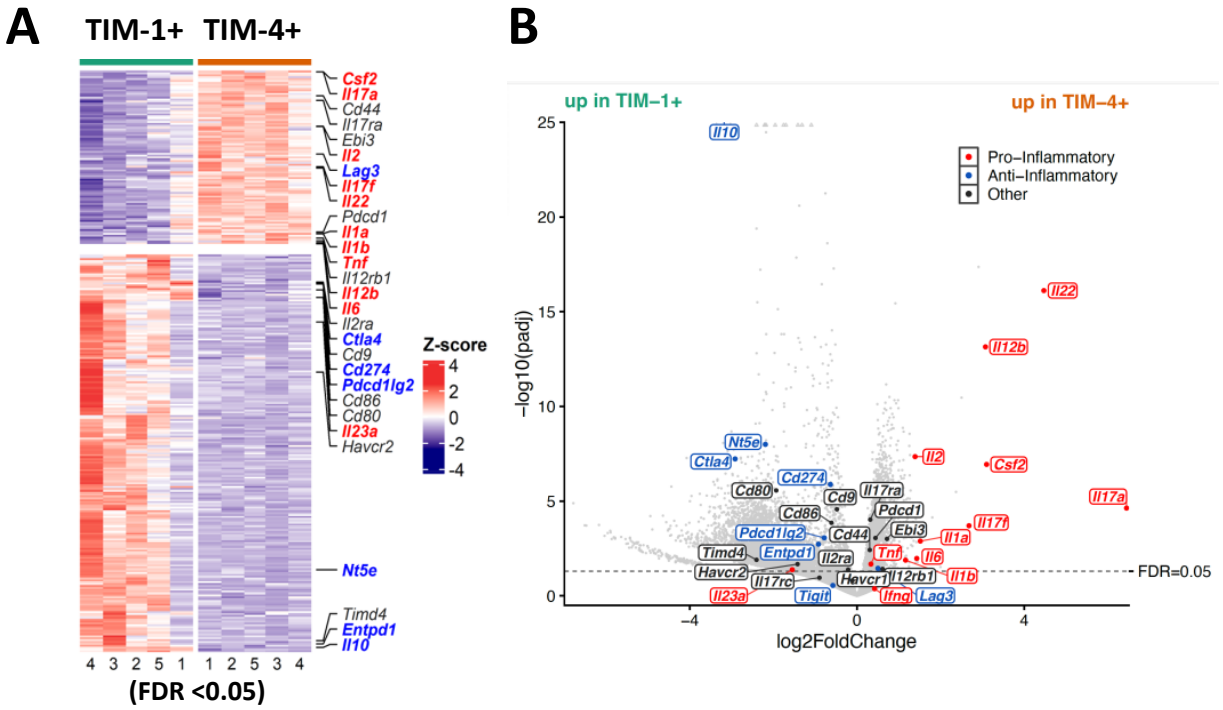

Up in TIM-4+: 3425 genes (613 with FC>1.5)
Down in TIM-4+: 7858 genes (7393 with FC > 1.5)

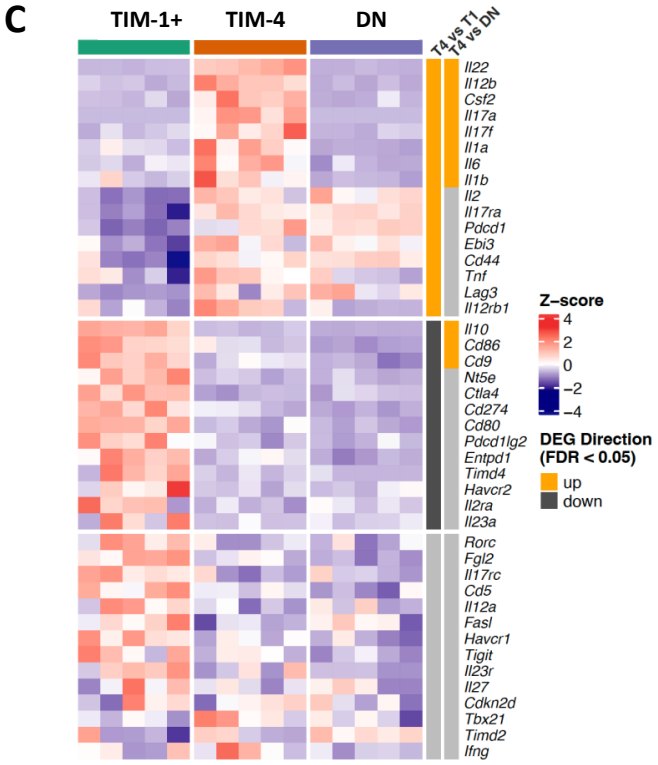

D

	Fold Change	
Gene	**TIM-4+ vs TIM-1+**	**TIM-4+ vs all TIM-4-**
Il17a	87.2	228.9
Il22	22.1	37.0
Il12b (p40)	8.4	11.5
Csf2 (GM-CSF)	8.6	9.2
Il17f	6.4	7.8
Il6	2.7	3.4
Il1b	2.2	3.0

Fig 5. Differential gene expression in TIM-1$^+$ and TIM-4$^+$ B cells from alloimmunized mice.

A-B: Amongst genes of interest, pro-inflammatory genes are depicted in red, anti-inflammatory genes are in blue, and other genes are in black text. **A**) Heatmap showing differentially expressed genes identified by RNA-seq (FDR<0.05). **B**) Volcano plot with selected genes of interest. The y-axis is capped at 25 for visual clarity. **C**) Heatmap comparing expression of selected genes of interest between three groups: TIM-1$^+$, TIM-4$^+$ and DN B cells annotated on the right. Vertical bars represent genes that are upregulated (orange), downregulated (black), or not statistically differentially expressed (gray, FDR $\geq$ 0.05) in a given comparison between TIM-4+ B cells (T4) and either TIM-1+ (T1) or DN B cells. **D)** Fold change in expression between select genes in TIM-4$^+$ vs. TIM-1$^+$ B cells or TIM-4$^+$ vs. all other (TIM-4$^-$) B cells. Data are representative of a second independent experiment comparing TIM-4$^+$ vs TIM-4$^-$ B cells.

Supplementary Figure 1:

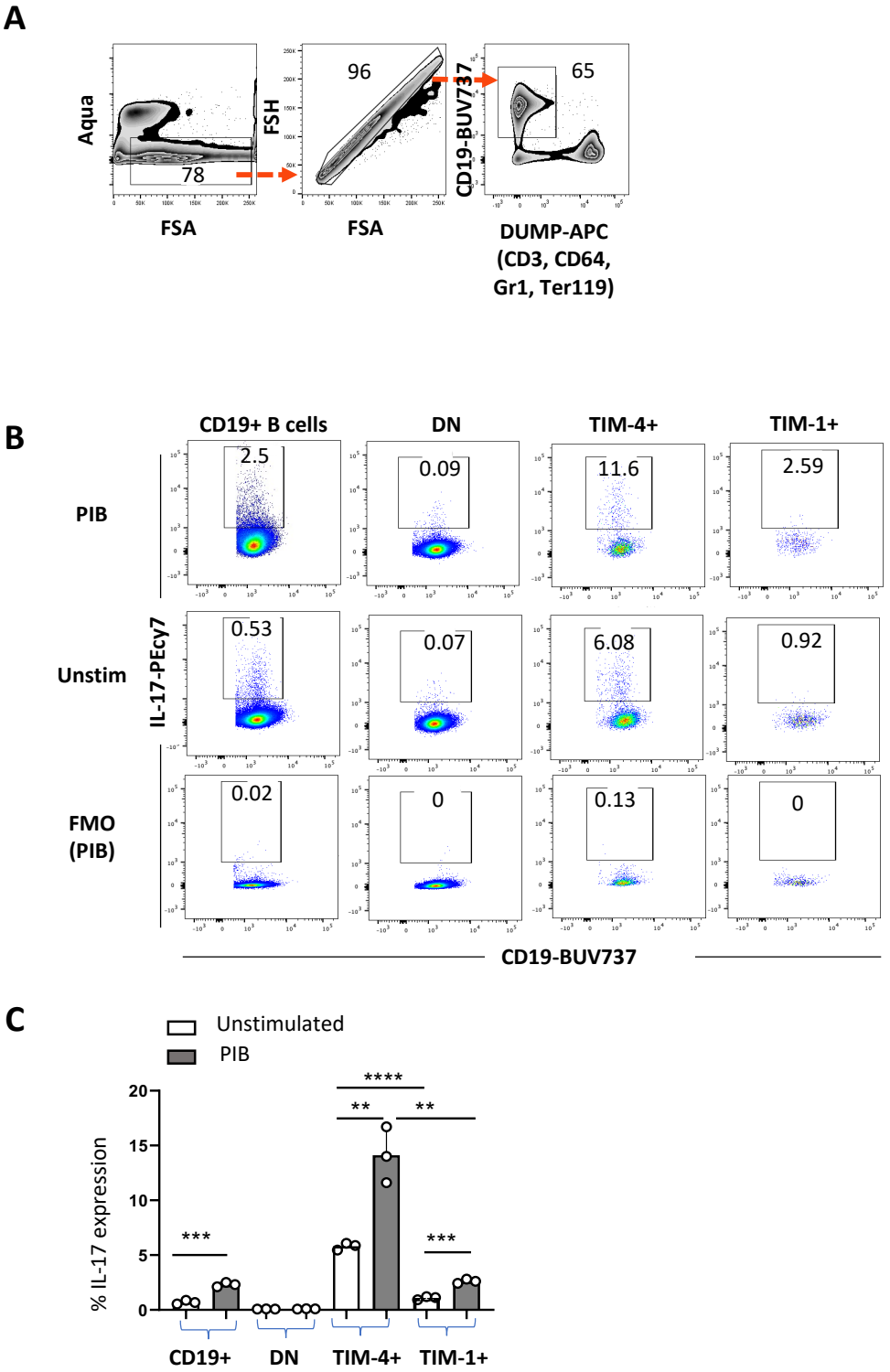

Supplementary Fig.1: Preferential IL-17A expression on TIM-4$^+$ B cells.

(A) Representative FACS plots for splenocytes from alloimmunized IL-17A-EGFP mice. Gating strategy for selection of CD19$^+$ Dump-gate (CD3, CD64, Gr1, Ter119) negative B cells assessed for IL-17A and TIM-4 expression in Figure 1E. (**B**) Representative FACS plots of IL-17A expression on total CD19$^+$ B cells, and TIM-1$^-$TIM-4$^-$ (DN), TIM-1$^+$, and TIM-4$^+$ B cell subpopulations from spleens from mice 14 days after immunization with MOG_{35-55}, CFA, and pertussis toxin to induce EAE (unstimulated vs. PIB for 5 hours). **(C)** Bar graph showing mean frequency (+ SD) of IL-17A expression by the B cell subpopulations shown in **(B)** (n≥3 mice per group). **p <0.01, ***p<0.001, ****p<0.0001 versus indicated groups.

Supplementary Figure 2:

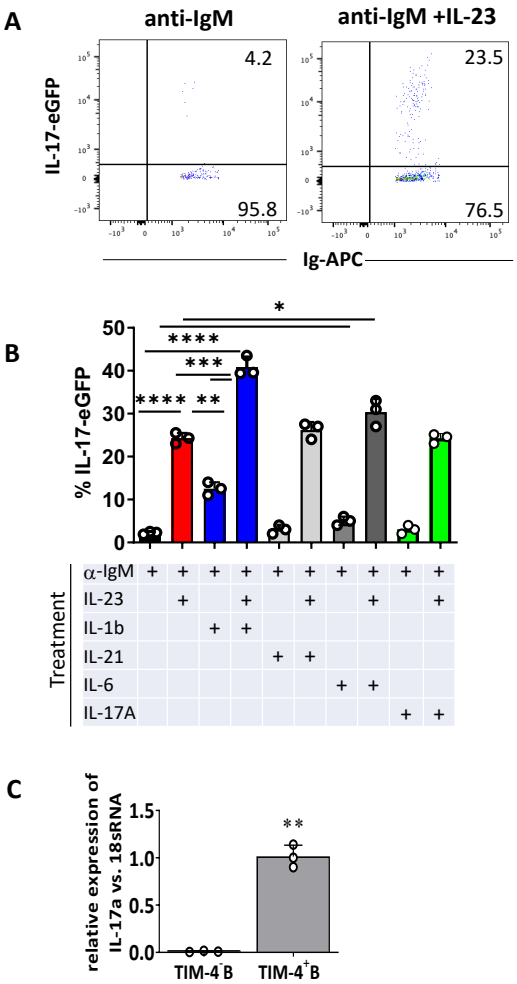

Supplementary Fig.2 IL-17A expression by TIM-4⁺ B cells is increased by IL-23.

A-B: Splenocytes from IL-17-EGFP mice were stimulated with anti-IgM and various cytokines for 24 hours and B cell IL-17A (EGFP) expression was assessed by flow cytometry ($CD19^+Sca1^+$ gate). (**A**) Representative flow cytometry plots showing IL-17A expression on anti-IgM vs. anti-IgM + IL-23-stimulated splenic B cells. (**B**) Mean frequency (+SD) of IL-17A expression after anti-IgM + cytokines, as indicated. statistical significance: *p<0.05; ** p<0.01; *** p<0.001; **** p<0.0001. **(C)** Bar graph of IL-17A mRNA expression by sort-purified TIM-4^+ and TIM-4^- B cells by qPCR (expressed as $2^{\wedge\Delta\Delta}Ct$ relative to expression 18s RNA) after stimulation with anti-IgM $^+$ IL-23 for 24 hours. PMA plus ionomycin were added for the final 3 hours. Samples run in duplicate and representative of 3 independent experiments (** p<0.01).

Supplementary Figure 3

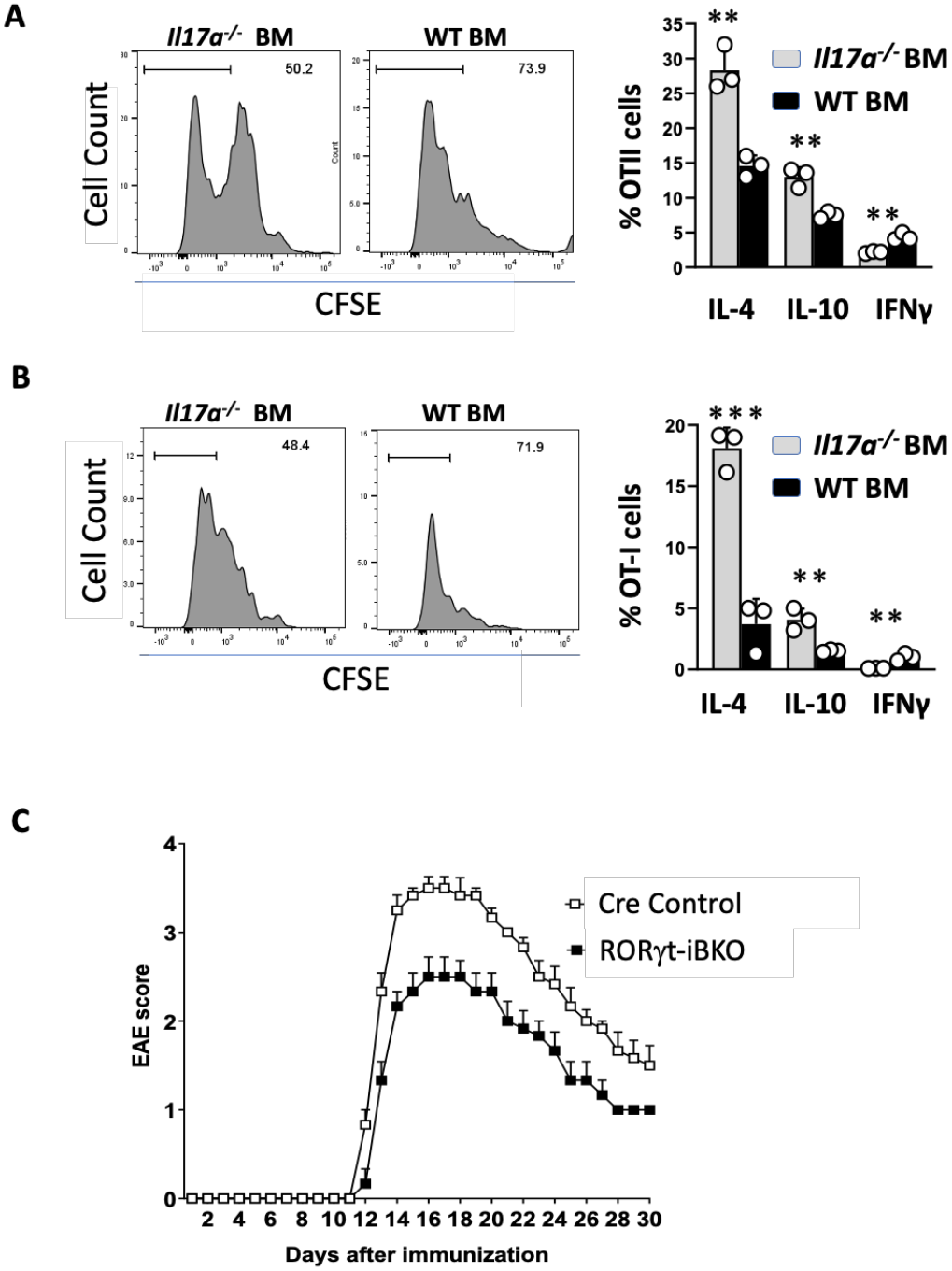

Supplementary Figure 3

D

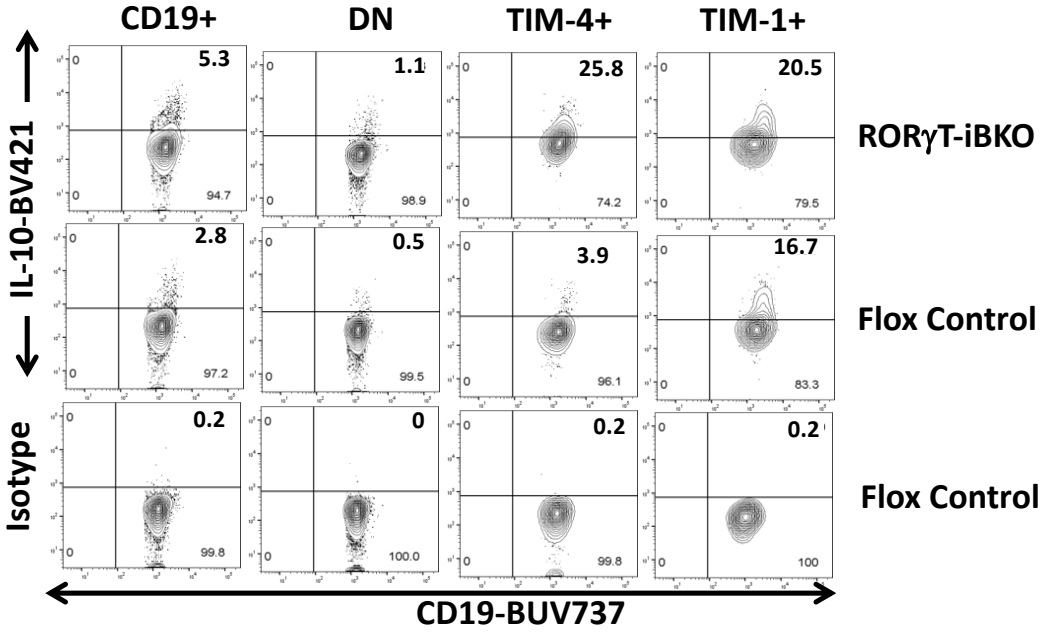

Supplementary Fig.3: The Role of B cell IL-17 and RORγt on the immune response.

A and B: BM chimeras were generated as in **Fig 2F**, by reconstituting lethally irradiated µMT mice with either 80% µMT plus 20% either *Il17a*$^{-/-}$ or WT bone marrow. After 8 weeks, BM chimeras were immunized with mitomycin C-treated splenocytes from Act-OVA.BALB/cXB6 F1 mice followed by adoptive transfer of 2×10^6 CFSE-labeled CD90.1$^+$ OT-II CD4$^+$ **(A)** or CD90.1$^+$ OT-I CD8$^+$ T cells **(B)**. Transferred (CD90.1$^+$) OT cells in spleen from the recipient mice were analyzed by flow cytometry for proliferation by CFSE dilution (day 4; Left panels), and intracellular cytokines expression (day 7; Right panels). n=3 mice per group. *p <0.05, **p <0.01 **(C)** Tamoxifen-treated RORγt-iBKO and Cre control mice were immunized to induce EAE and monitored daily for clinical signs (n=8-10 mice/group). Differences in clinical score was assessed using 2-way ANOVA (****p < 0.0001). **(D)** Representative flow cytometry plots show IL-10 expression (Intracellular staining after LPIM stimulation) on total CD19$^+$ B cells, and TIM-1$^-$TIM-4$^-$ DN, TIM-1$^+$ and TIM-4$^+$ B cell subpopulations from spleens of tamoxifen-treated alloimmunized RORγt-iBKO and Flox control mice.

Supplementary Figure 4

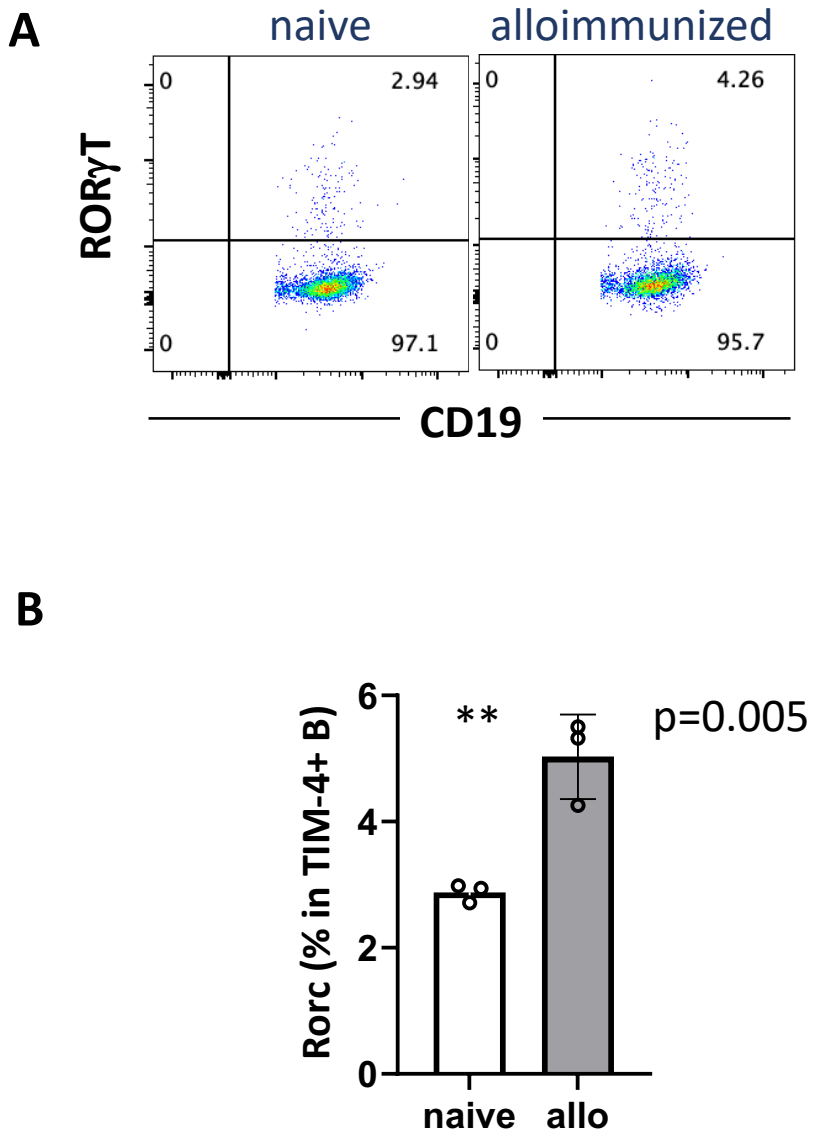

Supplementary Fig.4: RORγt expression on CD19⁺ TIM-4⁺ B cell subpopulations from spleens from alloimmunized wt B6 mice

(A) Representative FACS plots of RORγt expression on CD19⁺ TIM-4⁺ B cell subpopulations from spleens from alloimmunized wt B6 mice. **(B)** Bar graph showing mean frequency (+ SD) of RORγt expression by the B cell subpopulations shown in **(A)** (n=3 mice per group). **p <0.01.

Supplementary Fig.5

A Principal Component Analysis

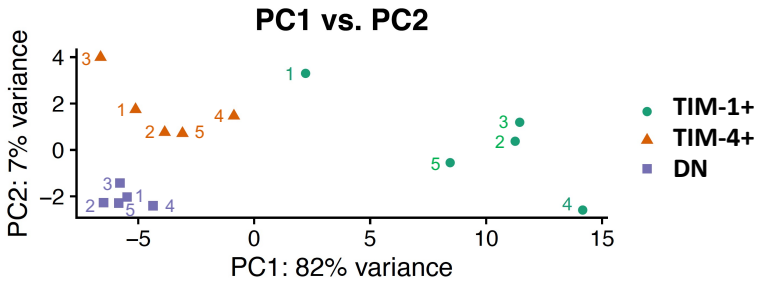

B Cytokine expression by intracellular staining

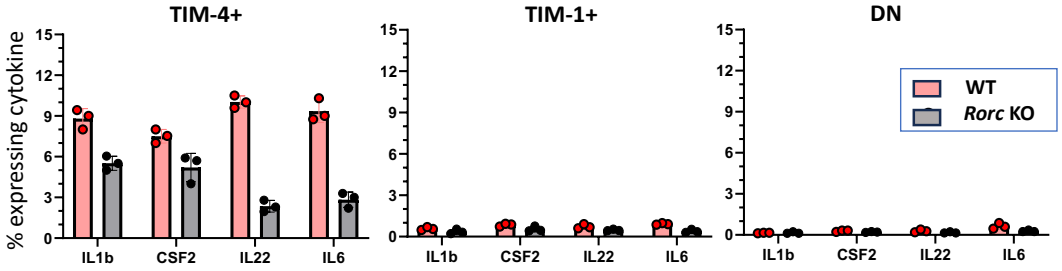

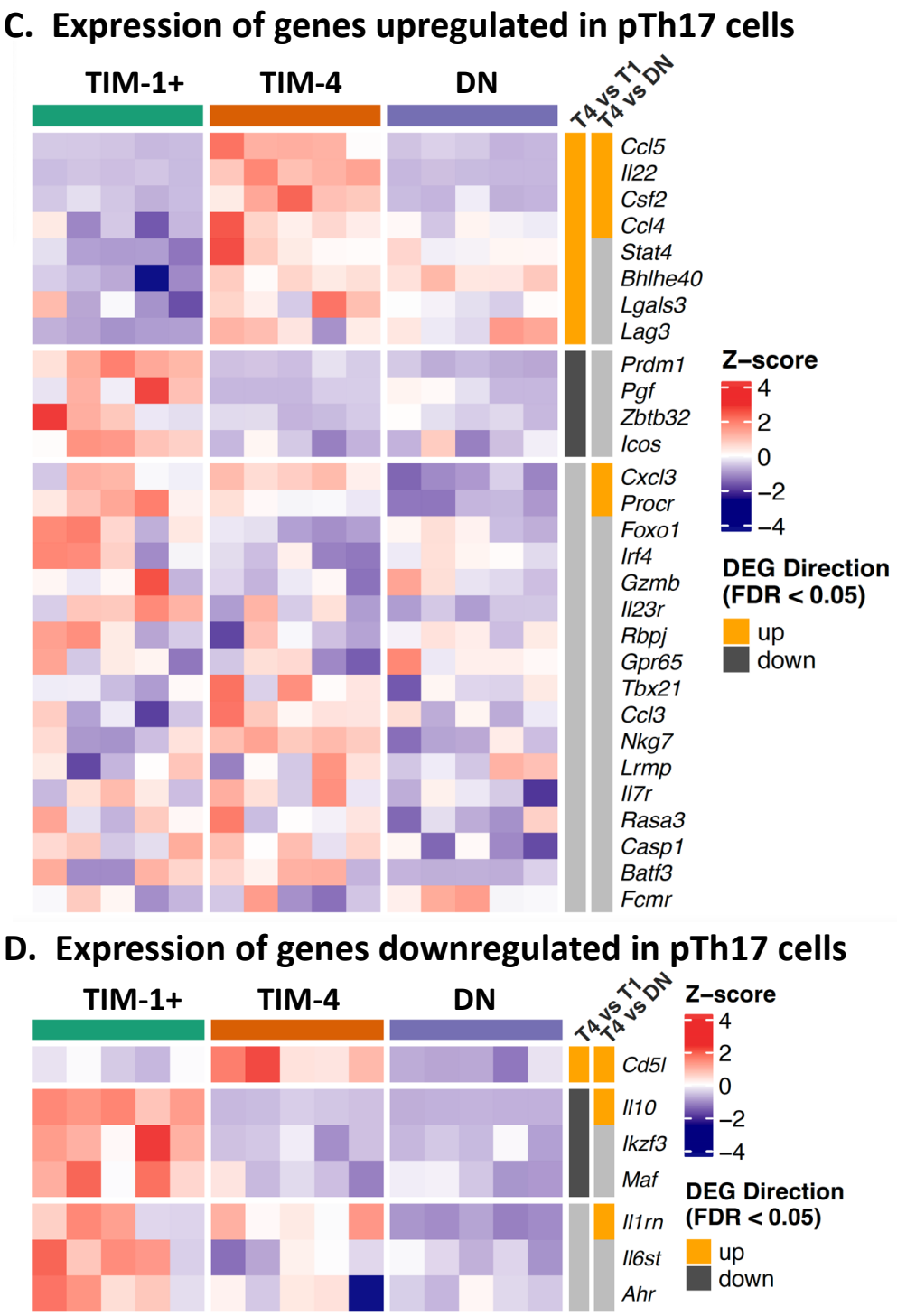

Supplementary Fig.5: Gene expression in TIM-1$^+$, TIM-4$^+$, and DN B cells.

(A) Principal Component Analysis (PCA) reveals TIM-1$^+$, TIM-4$^+$, and DN B cells comprise 3 distinct cell populations. PCA plot derived from bulk RNA-seq showing the relationship between the gene expression profiles of TIM-1$^+$TIM-4$^-$CD19$^+$, TIM-4$^+$TIM-1$^-$CD19$^+$, and TIM-1$^-$TIM-4$^-$CD19$^+$ (DN) B

cells from day 14 alloimmunized mice stimulated with anti-IgM plus IL-23 (24 hours) and PMA and ionomycin (3 hours). Each point represents a sample from an individual mouse, labelled (1-5) according to corresponding mouse. **(B)** Bar graph showing mean frequency (+SD) of IL-1β, CSF2, IL-22 and IL-6 expression on TIM-4^{+}, TIM-1+ and DN B cells from alloimmunized IL-RORγT$^{-/-}$ versus WT B6 mice, n = 3 mice/group. **(C,D)** Heatmaps showing comparison of gene expression assessed by RNA-seq for genes identified as being upregulated (**C**) or downregulated (**D**) in pTh17 cells (pTh17 signature) in various publications [23,25-29]. Genes that are differentially expressed (FDR <0.05) between TIM-4+ B cells and either TIM-1+ B cells or DN B cells are color coded (orange for up-regulated and black for down-regulated; gray if not statistically significant) by corresponding vertical lines at the right of each heatmap. The gene expression values are row normalized (z-score).

Supplementary Table 1: Top 50 s TIM-4+ vs. TIM-1+ B cells

Up in TIM-4+ B Cells

rank	gene_id	gene_symbol	baseMea	log2FoldCh	lfcSE	pvalue	padj
1	ENSMUSG00000035042	Ccl5	72.06771943	2.906021532	0.315113587	3.46E-21	4.31E-18
2	ENSMUSG00000074695	Il22	28.70990426	4.467818922	0.497063285	7.41E-20	7.68E-17
3	ENSMUSG00000059743	Fdps	597.155691	0.91668233	0.10328596	3.79E-19	3.62E-16
4	ENSMUSG00000004296	Il12b	34.46391266	3.071568534	0.380255352	1.07E-16	7.19E-14
5	ENSMUSG00000051022	Hs3st1	882.4770226	0.696953162	0.091329791	1.61E-14	6.91E-12
6	ENSMUSG00000029730	Mcm7	1668.080192	0.773811177	0.104521252	8.28E-14	3.17E-11
7	ENSMUSG00000029581	Fscn1	40.72645384	2.499524318	0.349185901	9.12E-14	3.44E-11
8	ENSMUSG00000079227	Ccr5	847.9478436	0.894921885	0.122182669	1.28E-13	4.74E-11
9	ENSMUSG00000027203	Dut	555.0948578	0.982190897	0.134372418	1.31E-13	4.74E-11
10	ENSMUSG00000020739	Nup85	520.9600182	0.677709852	0.09262463	1.8E-13	6.4E-11
11	ENSMUSG00000023004	Tuba1b	4168.43721	0.935728918	0.12887592	1.96E-13	6.85E-11
12	ENSMUSG00000089809	Rasgef1b	2588.378351	0.485528571	0.066375251	2.22E-13	7.57E-11
13	ENSMUSG00000026355	Mcm6	2927.492418	0.802657501	0.111619546	3.86E-13	1.24E-10
14	ENSMUSG00000028832	Stmn1	726.0987242	0.990060847	0.138303935	3.9E-13	1.24E-10
15	ENSMUSG00000040681	Hmgn1	1789.154918	0.658657447	0.091452532	4.18E-13	1.32E-10
16	ENSMUSG00000002870	Mcm2	1302.273229	0.69781411	0.097356849	5.23E-13	1.57E-10
17	ENSMUSG00000078193	Gm2000	2693.799963	0.628477772	0.088231252	7.75E-13	2.27E-10
18	ENSMUSG00000079197	Psme2	829.7571014	0.842597973	0.119079643	8.63E-13	2.5E-10
19	ENSMUSG00000022186	Oxct1	801.1391558	0.872546201	0.124393173	1.34E-12	3.75E-10
20	ENSMUSG00000038644	Pold1	426.6718181	0.77681008	0.110708919	1.43E-12	3.91E-10
21	ENSMUSG00000032604	Qars	955.923971	0.496957702	0.070864521	1.95E-12	5.21E-10
22	ENSMUSG00000027342	Pcna	2454.278688	0.744167692	0.107115436	2.32E-12	5.95E-10
23	ENSMUSG00000063229	Ldha	1318.795057	0.831724153	0.121114799	3.81E-12	9.2E-10
24	ENSMUSG00000021273	Fdft1	664.6699837	0.722071408	0.104866364	3.86E-12	9.24E-10
25	ENSMUSG00000020949	Fkbp3	558.4208272	0.637961721	0.092819533	4.63E-12	1.08E-09
26	ENSMUSG00000040212	Emp3	188.2811675	1.094863193	0.162047715	5.96E-12	1.36E-09
27	ENSMUSG00000001525	Tubb5	10537.40113	0.85225576	0.125529004	6.37E-12	1.43E-09
28	ENSMUSG00000027447	Cst3	292.1813802	0.873948106	0.128794445	6.39E-12	1.43E-09
29	ENSMUSG00000062647	Rpl7a	8491.929193	0.507633737	0.074447505	6.62E-12	1.47E-09
30	ENSMUSG00000024640	Psat1	1581.08949	0.81074963	0.119681667	7.47E-12	1.63E-09
31	ENSMUSG00000005410	Mcm5	1751.640074	0.749890709	0.110934574	8.9E-12	1.91E-09
32	ENSMUSG00000060600	Eno3	231.2771357	1.113705369	0.166957314	1.04E-11	2.16E-09
33	ENSMUSG00000020917	Acly	1810.919915	0.544805748	0.08027555	1.2E-11	2.47E-09
34	ENSMUSG00000069302	Hist1h2ah	455.0589581	1.256735717	0.190380264	1.37E-11	2.79E-09
35	ENSMUSG00000015937	H2afy	882.8741456	0.521313879	0.077589281	1.5E-11	3.01E-09
36	ENSMUSG00000025630	Hprt	1035.787993	0.616020885	0.092308561	1.98E-11	3.87E-09
37	ENSMUSG00000029283	Cdc7	170.022961	0.810919707	0.12279481	2.41E-11	4.62E-09
38	ENSMUSG00000062070	Pgk1	1903.90246	0.681880715	0.103594458	3.31E-11	6.24E-09
39	ENSMUSG00000074403	Hist2h3b	1518.964476	0.98101995	0.15062903	3.51E-11	6.57E-09
40	ENSMUSG00000003868	Ruvbl2	899.8679741	0.615940047	0.094068676	4.17E-11	7.74E-09
41	ENSMUSG00000030268	Bcat1	1630.372225	0.552235749	0.084720961	5.74E-11	1.03E-08
42	ENSMUSG00000035455	Fignl1	389.050945	0.942821832	0.146315914	5.96E-11	1.06E-08
43	ENSMUSG00000071644	Eef1g	9217.331127	0.502980046	0.078083086	6.02E-11	1.06E-08
44	ENSMUSG00000021895	Arhgef3	832.9001089	0.571080781	0.08783889	6.2E-11	1.09E-08
45	ENSMUSG00000027597	Ahcy	1493.770023	0.790430652	0.122353088	7.03E-11	1.18E-08
46	ENSMUSG00000069308	Hist1h2bp	362.9598842	1.249676395	0.196868015	7.4E-11	1.22E-08
47	ENSMUSG00000026192	Atic	559.2587497	0.665916756	0.103152065	7.65E-11	1.25E-08
48	ENSMUSG00000025428	Atp5a1	5454.0826	0.577800758	0.089620831	8.74E-11	1.39E-08
49	ENSMUSG00000028798	Eif3i	1746.788995	0.566757325	0.08877663	1.34E-10	2.04E-08
50	ENSMUSG00000056091	St3gal5	202.3775946	0.962136185	0.152315292	1.35E-10	2.04E-08

Down in TIM-4+ B Cells

rank	gene_id	gene_symbol	baseMea	log2FoldCh	lfcSE	pvalue	padj
1	ENSMUSG00000016529	Il10	373.6124808	-3.174926696	0.193322341	1.04E-61	2.59E-57
2	ENSMUSG00000024399	Ltb	114.3665082	-3.029783767	0.198917194	2.3E-53	2.86E-49
3	ENSMUSG00000002985	Apoe	1302.452635	-3.361989513	0.225191432	1.67E-51	1.38E-47
4	ENSMUSG00000091971	Hspa1a	673.7633919	-2.17620323	0.148252752	1.13E-49	7.03E-46
5	ENSMUSG00000004110	Cacna1e	196.3467818	-1.957577369	0.140572865	6.52E-45	3.25E-41
6	ENSMUSG00000090877	Hspa1b	691.53557	-2.211713321	0.162067134	2.74E-43	1.14E-39
7	ENSMUSG00000022708	Zbtb20	599.9521867	-1.414312584	0.10387461	9.41E-43	3.34E-39
8	ENSMUSG00000048031	Fcrl5	93.61291773	-2.403526407	0.179756412	1.27E-41	3.94E-38
9	ENSMUSG00000030256	Bhlhe41	324.3327125	-1.701774232	0.129678695	4.95E-40	1.37E-36
10	ENSMUSG00000041268	Dmxl2	126.4302072	-2.205066042	0.172202678	2.11E-38	5.09E-35
11	ENSMUSG00000023034	Nr4a1	2228.952279	-1.094673798	0.084967463	2.25E-38	5.09E-35
12	ENSMUSG00000051457	Spn	253.8398536	-1.756803171	0.151999016	1.24E-31	2.58E-28
13	ENSMUSG00000019820	Utrn	240.4539032	-1.315676072	0.116252245	3.3E-30	6.31E-27
14	ENSMUSG00000005397	Nid1	83.81502284	-2.17618734	0.199925756	1.89E-28	3.36E-25
15	ENSMUSG00000024789	Jak2	4358.129484	-0.756614488	0.073688821	3.41E-25	5.66E-22
16	ENSMUSG00000092274	Neat1	582.9467038	-1.381833217	0.13692147	1.62E-24	2.52E-21
17	ENSMUSG00000026604	Ptpn14	60.25103016	-2.404412171	0.247134621	2.79E-23	4.08E-20
18	ENSMUSG00000033730	Egr3	1652.561786	-0.710197188	0.073125896	1.75E-22	2.42E-19
19	ENSMUSG00000096054	Syne1	234.9408171	-1.451584647	0.154004847	1.06E-21	1.39E-18
20	ENSMUSG00000028341	Nr4a3	4882.869898	-0.558182192	0.059396146	4.41E-21	5.22E-18
21	ENSMUSG00000097636	Mirt1	70.13065376	-2.31358269	0.251702876	5.37E-21	6.07E-18
22	ENSMUSG00000018476	Kdm6b	6574.513492	-0.843185215	0.092143454	3.26E-20	3.53E-17
23	ENSMUSG00000073802	Cdkn2b	39.94674346	-2.385092463	0.272735786	3.21E-19	3.19E-16
24	ENSMUSG00000015968	Cacna1d	67.83243961	-1.893982313	0.218753185	7.99E-19	7.36E-16
25	ENSMUSG00000019943	Atp2b1	1384.76916	-0.600238413	0.07036234	1.08E-17	9.6E-15
26	ENSMUSG00000022197	Pdzd2	105.7698387	-1.808309946	0.21780993	1.82E-17	1.53E-14
27	ENSMUSG00000033060	Lmo7	47.35585259	-2.172451331	0.262477851	1.9E-17	1.53E-14
28	ENSMUSG00000025279	Dnase1l3	92.33061135	-1.744049275	0.210080672	1.91E-17	1.53E-14
29	ENSMUSG00000030790	Adm	233.7529412	-1.006921067	0.120410575	2.86E-17	2.22E-14
30	ENSMUSG00000021728	Emb	147.2953846	-1.403478584	0.169426906	3.25E-17	2.45E-14
31	ENSMUSG00000025429	Pstpip2	114.5665404	-1.367533856	0.166198704	5.69E-17	4.16E-14
32	ENSMUSG00000030287	Itpr2	968.6899376	-0.73866682	0.089178245	7.61E-17	5.4E-14
33	ENSMUSG00000027660	Skil	3955.572044	-0.518882224	0.062457322	7.81E-17	5.4E-14
34	ENSMUSG00000028649	Macf1	3792.206566	-0.864153806	0.104969881	1.11E-16	7.26E-14
35	ENSMUSG00000005364	Il5ra	126.4538882	-1.331770092	0.164241922	1.52E-16	9.68E-14
36	ENSMUSG00000041540	Sox5	49.69445624	-1.972697473	0.247427343	2.42E-16	1.5E-13
37	ENSMUSG00000079190	AC133103.1	45.85778417	-2.402714895	0.302424857	2.57E-16	1.56E-13
38	ENSMUSG00000071757	Zhx2	1155.864613	-0.639091974	0.078590293	2.99E-16	1.77E-13
39	ENSMUSG00000039219	Arid4b	1180.364832	-0.601828456	0.074859511	6.58E-16	3.81E-13
40	ENSMUSG00000015143	Actn1	239.4782173	-0.81975016	0.102935788	9.75E-16	5.51E-13
41	ENSMUSG00000050600	Zfp831	88.32603285	-1.636244948	0.209325627	1.1E-15	6.08E-13
42	ENSMUSG00000026872	Zeb2	1394.522768	-0.68582533	0.086255355	1.25E-15	6.75E-13
43	ENSMUSG00000003849	Nqo1	137.9338557	-1.179930638	0.150445925	1.62E-15	8.56E-13
44	ENSMUSG00000031709	Tbc1d9	66.42956458	-1.470838654	0.188713259	1.72E-15	8.93E-13
45	ENSMUSG00000056888	Glipr1	145.2222802	-1.475133934	0.190990811	2.81E-15	1.43E-12
46	ENSMUSG00000092341	Malat1	44922.80992	-0.706226498	0.089921298	3.78E-15	1.88E-12
47	ENSMUSG00000051111	Sv2c	39.84954285	-2.351891778	0.309501122	4.16E-15	2.03E-12
48	ENSMUSG00000044827	Tlr1	133.6359619	-1.062327486	0.137520334	4.83E-15	2.31E-12
49	ENSMUSG00000020178	Adora2a	180.6230609	-1.033547256	0.134700944	7.41E-15	3.48E-12
50	ENSMUSG00000036391	Sec24a	1066.507837	-0.607633343	0.078706289	9.28E-15	4.28E-12